FINAL REPORT

SUBMITTED TO:	National Aeronautics and Space Administration Langley Research Center Hampton, Virginia 23665
INSTITUTION:	Department of Physics and Engineering Studies Hampton Institute Hampton, Virginia 23668
TITLE OF GRANT:	Local Effects of Partly-Cloudy Skies on Solar and Emitted Radiation
GRANT NUMBER:	NAG 1-87
PERIOD COVERED BY THIS REPORT:	August 1, 1980 to July 31, 1983
CO-PRINCIPAL INVESTIGATORS:	D. A. Whitney D. D. Venable
RESEARCH ASSOCIATES:	T. J. Griffin J. R. Foreman

LOCAL EFFECTS OF PARTLY-CLOUDY SKIES ON SOLAR AND EMITTED RADIATIONS - FINAL REPORT

D. A. Whitney
T. J. Griffin
J. R. Foreman

Department of Physics and
Engineering Studies

ABSTRACT

The third year of the proposed three year project has now elapsed. The computer automated data acquisition system for atmospheric emittance, and global solar, downwelled diffuse solar, and direct solar irradiances has been fully operational for about two and one-half years. Hourly-integrated global solar and atmospheric emitted radiances have been measured continuously from February 1981 to August 1983. Hourly-integrated diffuse solar and direct solar irradiances have been measured continuously from October 1981 to August 1983. One-minute integrated data have been made available for each of these components from February 1982 to August 1983.

Atmospheric aerosol and turbidity measurements for the period February 1981 through July 1983 have been analyzed and the results are presented here.

The correlation of global insolation with cloud cover fractions for the first complete year's data set was completed. A theoretical model was developed to parameterize the effects of local aerosols upon insolation received at the ground using satellite radiometric data and insolation measurements under clear sky conditions. A February data set, composed of one-minute integrated global insolation and direct solar irradiances, cloud cover fractions, meteorological data from nearby weather stations, and GOES East satellite radiometric data was collected to test the model and used to calculate the effects of local aerosols.

TABLE OF CONTENTS

INTRODUCTION

A solar energy measurement station was established at Hampton Institute, February 15, 1981. Routine hourly integrated measurements were made of global, diffuse, and direct solar irradiances and of atmospheric emittance. After the data acquisition was computer automated in February 1982, one-minute integrated radiometric data, as well as one-hour integrated data, were recorded. More detailed information about the measurement system is presented in Sections I and II of this report. Monthly averages for global, diffuse, and direct solar irradiance, atmospheric emittance, and atmospheric aerosol and turbidity parameters were calculated and are presented in Section III.

Correlation of global insolation with cloud cover fractions were made using the ARL model and the results for the first complete year of data are presented in Section III. A parameterization method for estimation of the effect of aerosols upon insolation has been developed and a data set has been accumulated to test this method. Detailed information about the parameterization method is provided in Section IV.

I. SOLAR RADIATION MEASUREMENT PROGRAM

An observation platform for solar and atmospheric radiation measurements was established on the roof of Turner Hall (latitude 37.02°N, longitude 76.34°W, and elevation 24 meters) February 15, 1981. A radio tower and a smokestack are the only two obstructions greater than ten degrees above the horizon with all other obstructions less than five degrees above the horizon. Routine measurements were made of global solar irradiance, diffuse solar irradiance, direct solar irradiance, and atmospheric emittance. Information (Griffin, 1982) about the solar radiation measurement program was presented at the April 20-23, 1982 meeting of the Virginia Academy of Science held in Blacksburg, Virginia and at the June 1-3, 1983 meeting of the American Solar Energy Society in Minneapolis, Minnesota (Whitney, 1983). The Abstract of the presentations by T. J. Griffin are attached as Appendices I and II. A summary of the solar and atmospheric data available at the time of this report is provided in TABLE I.

A. Instrumentation

Since detailed descriptions of the radiometric instrumentation are available in the first Annual Report (Whitney, 1981) for this grant, only a summary of our measurement capabilities is presented here. The global solar irradiance on a horizontal surface was measured by an Eppley Precision Spectral Pyranometer (PSP) with a hemispherical WG7 Schott glass dome. Diffuse solar irradiance on a horizontal surface was measured by an Eppley PSP with a WG7 dome that was mounted on an Eppley Solar Tracker and Occulting Disk System. Direct solar irradiance was measured by an Eppley Normal Incidence Pyrheliometer (NIP) mounted on a Solar Tracker. An Eppley Hickey-Frieden Absolute Cavity Pyrheliometer was used to calibrate the NIP regularly. Atmospheric emittance was measured with an Eppley Precision Infrared Radiometer (PIR). In addition, turbidity (Volz, 1974) measurements were made approximately hourly for clear

sky conditions using a Volz Sunphotometer.

The wavelength range of each of these instruments is listed in Table II. Information about the measurement frequency and about the time periods that insolation data are available is presented in TABLE I.

B. Calibration

Each radiometer was calibrated prior to delivery by the manufacturer. Subsequent calibrations have been performed by comparison to secondary or primary standards at Hampton Institute or at Eppley Laboratory. Calibration data are presented in TABLE III by listing each instrument, the date and site of each calibration and the calculated sensitivity factor. The NIP was calibrated by comparison to the Hickey-Frieden Absolute Cavity Pyrheliometer which is considered to be a primary standard. There were no adjustments in the NIP calibration factor since the calculated sensitivity showed no change within the sensor accuracy. The pyranometers were compared twice a year with one another by comparison of three-day integrated global irradiance totals after side-by-side operation. Comparison between the pyranometers indicated a consistent difference of about one percent which was within the two percent accuracy of each instrument, thus no adjustment in either calibration factor was necessary. A list of equipment used in these calibrations is attached as Appendix III.

The pyrgeometer (PIR) and the pyranometers were recalibrated at Eppley Laboratory twice during the three-year period of use. A change in calibration standards at Eppley Laboratory in October 1981 accounted for a 2.6 percent change in sensitivity factor for the PSP instruments, and required that data obtained previous to that date be adjusted to standardize our data set. Annual calibrations of both PSP's at Eppley Laboratory showed a sensor degradation in each instrument of approximately 0.1% per month. A linear correction factor between Eppley calibrations for each instrument has been

calculated and used for the monthly average measurements presented in this report. Raw data stored on magnetic tape have not been corrected for the above changes in sensor sensitivity. Monthly correction factors used to adjust all of the raw data on tape are presented in TABLE IV for each radiance component.

The recorder systems were calibrated every six months by using a stable millivolt source and by adjusting the integrator and strip chart recorder gains to obtain the proper readings. The electronic integrators exhibited extreme stability with the maximum adjustment required for any integrator being only 0.4%, while larger adjustments were occasionally required for the chart recorders.

The meter on the Volz Sunphotometer was replaced on April 29, 1983 immediately after it became inoperative. Telephone discussions with the manufacturer revealed that the change in meter would have a negligible effect on the calibration of the instrument. An attempt to verify this by checking for linearity of the sensor on a Langley Plot of meter readings versus air mass failed due to an inability to obtain enough clear sky measurements on a given day over a significant range in air mass. Atmospheric aerosol and turbidity data reported in this report have been calculated using the original calibration data.

C. Meteorological Data

Standard hourly meteorological observations taken at nearby Langley Air Force Base (LAFB) were picked up on a monthly basis from Detachment 7, Third Weather Squadron and are on file at Hampton Institute. These data included information about cloud height, cloud type, fractional sky cover, precipitation, sea level pressure, and temperature. These data were supplemented by whole-sky photographs and visual cloud observations at Hampton Institute. Additional meteorological, turbidity and ozone data were purchased from the National

Climatic Center archives in Asheville, North Carolina and the World Ozone Center, Environment Canada, Toronto, Canada for use in the data analysis.

D. Cloud Cover Fractions

Cloud cover composed of cumuliform clouds were selected for this study because of the nearly opaque optical properties, low cloud altitude, distinct boundaries, and frequency of occurence. Cloud cover fraction was defined for the local area as the ratio of cloudy area to the total area. There are three different sources of cloud cover fractions: 1) satellite data, 2) ground based photography, and 3) trained observers. Only a summary of these methods is provided here since details about the analysis methods are provided in the first Annual Report (Whitney, 1981). These cloud cover fractions were used in the ARL regression equation as discussed in Section III-C of this report. These methods are compared with one another in the first Annual Report.

1. Satellite Derived Cloud Cover Fractions

Black and white photoprints of visible imagery provided by GOES-EAST were selected on the bases of: 1) frequency (every one-half hour), 2) range of cloudiness (all fractions possible), and 3) convenience (our local geography was easily distinguishable in the prints). A distance scale was calculated from known landmarks on the photoprints for the east-west and north-south directions. Using this information an ellipse corresponding to a 120 km radius horizon circle was drawn on a clear plastic overlay. The ellipse was further subdivided into grids that corresponded to 24 km x 24 km squares at the ground. The central grid was placed over the Hampton Institute measurement site and visual estimates of cloud cover fractions made for each grid. These fractions were then used to calculate the cloud cover fraction for the local area. Comparison of the fractions obtained by this method to the other two methods indicated that the photoprint method was the least reliable for cumuliform clouds and, thus, satellite photoprint analysis was only used during the first year of this program.

2. Ground Based Photograph-Derived Cloud Cover Fractions

A whole-sky photographic system was constructed using a 35 mm SLR camera body, an Aetna fish-eye adaptor lens, and a camera mount directed toward zenith. The camera system was calibrated by aiming at a large flat surface (a classroom wall) and carefully measuring the radial distance on the photograph for each known angular position. A linear relationship was observed between angular position and radial distance in the photograph as indicated in Figure 1 from the center out to 85 degrees.

The 85.0 degree field of view about the zenith defines the local area as a circle of radius from 2 to 50 km depending on cloud altitude. Over this limited field of view the atmosphere can be treated as being flat and the cloud cover fraction can be calculated independent of cloud altitude. (See the first Annual Report for details). An analysis grid for ground based photographs and slides was developed using concentric rings and radial sectors. During the first year, black and white photographs were enlarged to fit the analysis grid overlay and a cloud cover fraction determined for each grid by visual inspection. Afterwards color slides were directly projected onto the analysis grid in order to aid in distinction between dark cloud bottoms and clear sky, and to reduce both processing and analysis times.

The whole-sky camera system was modified in order to allow computer activation of the camera by adding an electronic shutter and an autowind system. The camera system was mounted on the Eppley Shadow Band Stand in order to eliminate the need for frequent adjustment of the sunshade. A clock and date card were placed on the inside surface of the shadow band to document the time of day and date of each photograph. Whole-sky photographs (color slides) were taken every one-half hour on selected weekdays when clouds were present without precipitation, from August 1981 through December 1982.

3. Visual Observations of Cloud Cover Fraction

Visual estimates of cloud cover were made by trained observers at nearby Langley Air Force Base every hour. The observations included the cloud cover fraction in tenths and cloud type in code. These observations were screened to eliminate hours with predominantly transparent or semi-transparent clouds. Visual observations made at Hampton Institute during the first year were used in order to help interpret the photoprint and photograph analysis results.

E. Data Handling and Quality Control

A data storage procedure for the radiation data was devised to efficiently handle the data and ensure quality control. The integrated radiometric data and times were initially stored on a Tektronix 4051 microcomputer's internal magnetic tape unit. Then on a monthly basis these raw data files were transferred via computer hookup from the Tektronix 4051 to the PDP 11/34 minicomputer where the data were permanently stored on 1600 bpi magnetic tape. All preliminary processing was done on the Tektronix 4051, while data analysis routines and application programs were performed on the PDP 11/34 system. The data were examined for errors by a computer program that located the gaps in the data and identified places to be investigated and corrected.

The automated data acquisition system for global and direct solar irradiances was fully operational from February 1, 1982 through July 31, 1983. During that time integrated radiometric data for one-minute intervals were obtained directly from the Eppley integrators and stored on magnetic tape. Specific data handling procedures and quality control for these data are discussed in more detail in the next section of this report.

Prior to the installation of the automated data acquisition system, only one-hour integrated measurements were recorded on magnetic tape. Printed data from the integrators were scanned on a daily basis for missing or problem data and incorrect timing caused by power failures or other electrical and mechanical malfunctions. Missing data were supplemented by the strip chart record when available. Approximately once a week these data were manually entered into the Tektronix 4051 microcomputer, inspected for operator errors, and then transferred to the PDP 11/34 data storage tape.

II. AUTOMATED DATA ACQUISITION SYSTEM

One of the major objectives of the second year of this research project was to develop and implement an automated data acquisition system. This system reduced the manhour requirements, and the number of operator induced errors, involved with data transferral from the integrator-recording system to final permanent magnetic tape storage. The hardware requirements, operating procedures, features, and performance of the system were provided in the second Annual Report (Whitney, 1982) and are summarized below.

A. System Overview

The automated data acquisition system connected the radiometric sensor-integrator recording system with the microcomputer I/O capabilities via an interface box. The microcomputer read the integrated radiometric values from the BCD interface panels at a preset time interval and recorded these data on the internal magnetic tape unit. Whole-sky photographs were triggered by computer command at preset times and a record of time and picture number were recorded on the magnetic tape. Integrated atmospheric emittance, and global, direct, and diffuse solar irradiances were recorded at one-minute intervals from 0400 EST to 2000 EST and at ten-minute intervals for the rest of the night. The data for each month were transferred to separate 1600 bpi magnetic tapes for permanent storage.

B. System Description

The data acquisition system was composed of three separate subsystems:

(1) the radiometric sensor-integrator system;

(2) the integrated data sampling and recording system; and

(3) the data storage system.

A flow chart of the data acquisition system is presented in Figure 2. The radiometric sensor-integrator system is located at the top half of the chart and includes the following five components:

(1) the Eppley radiometers;

(2) the Eppley integrators that summed the instantaneous readings from the radiometers;

(3) the digitec printers that provided a hard copy printout of one-hour radiance values;

(4) the X-Y strip chart recorders that provided a hard copy of instantaneous radiances; and,

(5) the camera system that took the whole-sky photographs.

The integrated data sampling and recording system located at the lower left-hand side of the chart includes:

(1) the integrator signals that were provided at the BCD interface on the Eppley integrators;

(2) the interface box that centralized the data for computer access;

(3) the ROMs that interfaced the BCD data to the Tektronix 4051;

(4) the Tektronix 4051 microcomputer that read the ROMs and activated the camera photocounter; and,

(5) the magnetic tape cartridge where the computer stored the data.

The data storage system is located at the lower right-hand side of the chart and consists of three components:

(1) another Tektronix 4051 microcomputer with a RS232 interface that acted as a link between the PDP minicomputer and the internal tape of the Tektronix computer;

(2) the PDP 11/34 minicomputer system that read the data from the Tektronix 4051; and

(3) the 1600 bpi, 9 track magnetic tape for permanent storage of the data.

The hardware used in the integrated data acquisition and storage system are listed in Appendix IV along with two other devices that were used in the development and testing of the interface box and software programs. Detailed information about the operation of these devices and about the construction of the interface box is kept in a documentation file in the Solar Energy Measurement Laboratory.

C. Operating Procedure

The data acquisition system operated on the Tektronix 4051 microcomputer using the computer program SOLAUTO written in BASIC by D. D. Venable. The program worked by comparison of the time provided by the Real Time Clock ROM Pack with times that were calculated from fixed time intervals entered into the program for each sensor or for the camera system. A copy of the program listing is kept in the documentation file in the Solar Energy Measurement Laboratory. Basic operation of the data acquisition system was discussed in some detail in the second Annual Report.

The radiometric data were recorded on the magnetic tape in 72 character records. The first two-digit flag (Ø#) of the data record indicated the type of data string using: Ø1 for radiometric data, Ø2 for a photograph record, Ø3 for a user message, and Ø4 for a system message. The next characters indicated the day of the week (three letter abbreviation) separated by two spaces from the date in the form: day-month-year (DD-MMM-YY). The date was represented by two digits each for the day and for the year, and by the three letter abbreviation for the month. The next set of numbers (HH:MM:SS) in the data string were the time (EST) represented by two digits each for the hour, minute, and second, and the remaining characters were either a message or data. A radiometric data record had the form:

Ø1, DDD DD-MMM-YY HH:MM:SS, GL#,NNNNN,DF#,NNNNN,IR#,NNNNN,DR#,NNNNN

The radiometric data were recorded as integrated totals starting from zero at midnight using the two letter abbreviation for each radiation component, a single digit activation code (1 for on, Ø for off), and five digits for each reading (NNNNN). Global solar irradiance was abbreviated by GL: diffuse solar by DF: infrared (atmospheric emittance) by IR: and direct solar by DR.

D. System Performance

The performance of the computer automated data acquisition system was measured by calculation of the amount of data lost in comparison with the data recovered on magnetic tape. The performance record of the previous data acquisition system was also considered since both systems had some of the same causes for loss of data. For example, diffuse solar radiometric data were not collected during calibration periods for either pyranometer in 1982. Intercomparison of the pyranometers was made only for the horizontal global solar orientation. Electrical storms interfered with computer program execution and occasionally stopped data collection until the system was restored to normal operation. Severe storms reset the printer times and the integrator count values, an effect that destroyed the printer data until the system could be restored to normal operation. The strip chart recorders were used to retrieve most of the hourly integrated data lost by computer failure. Mechanical solar tracking failures sometimes caused the loss of the direct and diffuse solar data.

The hourly integrated-data recovery record is presented in TABLE V for the full period of the insolation measurement program at Hampton Institute. TABLE VI contains one and ten minute integrated data recovery information for the first five months of automated data acquisition. The measurement interval for global and direct solar irradiances was set at one-minute starting at 0942 EST February 1, 1982. One-minute integrated data sampling

for the diffuse solar and atmospheric emittance began at 2038 EST, March 1, 1982 when the second half of the interface box was completed. On March 13, 1982 the sampling interval at night was changed to ten minutes (from 2000 EST to 0400 EST) in order to reduce computer tape storage requirements. One Tektronix Data Tape Cartridge is used to store approximately six and one-half (6½) days of insolation data.

Two parameters used to measure the performance of the automated data acquisition system were the average time period between failures and the average length of time lost for each error. These parameters were referred to as Meantime to Fail and Downtime per Error, respectively. The Mean Time to Fail was calculated by dividing the total possible number of data records by the number of failures and by the data record sampling rate (while the sampling rate was constant). The Downtime per Error was calculated by dividing the number of data records lost by the number of errors and by the sampling rate. The results of these measures of performance were reported (Blakey, 1982) at the 39th Joint Annual Meeting of the National Institute of Science and Beta Kappa Chi Scientific Society held in Washington, DC, March 17-20, 1982. Rody Blakey, an undergraduate assistant on this project, used the data obtained during the first month of computer automated data acquisition to calculate the Meantime to Fail and Downtime per Error. The results of his analysis were an average of 8.7 days between failures and an average of 6.7 hours downtime per error. The large downtime per error was caused by the two nighttime failures that stopped program execution for several hours until the system could be returned to normal the following working day. (Mr. Blakey received a Third Place Award for his paper in the Mathematics and Computer Science Section of the Meeting and one of two general awards given.) A copy of the abstract of his paper is attached to this report as Appendix V.

III. RADIOMETRIC AND METEOROLOGICAL DATA ANALYSIS

Several types of data analysis have been completed using the radiometric and meteorological data collected at Hampton Institute. The first type of analysis completed was the calculation of average values for the various measurements. A second type of analysis was required to treat the raw turbidity measurements in order to obtain useful parameters such as optical depths and precipitable water. Correlation of data with empirical formulae was a third type of analysis performed. Analyses involving satellite-derived radiometric data are discussed in Section IV as part of the parameterization method. The results of the other analysis methods used are discussed below.

A. Radiometric Data Presentation

Diurnal variability in the various solar insolation components as observed by comparison of the average hourly values for afternoons with values for mornings. Average daily global, diffuse, and direct solar irradiances and atmospheric emittance are listed in TABLE VII. Average hourly global, diffuse, and direct solar irradiances and atmospheric emittance are plotted for each month from July 1981 through June 1983 in Figure 3 through Figure 9. Diurnal variability is indicated by the lack of symmetry in these graphs. Seasonal variability can be seen by plotting global solar irradiance for clear sky days selected from each season such as is done in Figure 10. Plots can also be made for values averaged over shorter time intervals (one minute to sixty minutes).

B. Atmospheric Aerosol Extinction and Turbidity Data Results

Individual measurements obtained with the Volz Sunphotometer (serial number 492) were used to calculate aerosol optical depths and turbidity parameters using the formulation outlined in the second Annual Report and by Volz (1974). Monthly average aerosol extinction coefficients at 380 nm, 500 nm and 875 nm, along with turbidity coefficient β_o and wavelength exponent α_o are listed in TABLE VIII for the measurement period-March 1981 through June 1983. The number of days on which measurements were obtained for each month are listed also.

The annual pattern of the Ångström turbidity coefficient, β_o is graphically illustrated in Figure 11. As shown in the figure, β_o values peaked in the midsummer. A high value of β_o represents a high aerosol concentration in the local air mass. Atmospheric aerosols include dust, smoke, sea salts and other suspended particles. The aerosol concentration decreased in the autumn through the spring season as represented by the 1981 through May 1982 data on Figure 11, however, in November 1982, β_o values sharply increased instead of decreasing as expected. This increase is due to the effect of volcanic particles released into the stratosphere from the eruptions of El Chichon in April 1982. The global spreading of this volcanic dust cloud appears to have reached the Hampton Institute study region (37 °N, 76 °W) during the month of November 1982. A slight reduction in aerosol concentration occurred in December 1982 and in January 1983, but the normal annual overall reduction in aerosol concentration indicated by the September 1981 to May 1982 data did not materialize. In 1983 the monthly average β_o values generally increased through June. Aerosol extinction data at 380 nm, 500 nm and 875 nm showed a pattern similar to that illustrated by β_o throughout the measurement period.

The Ångström exponent, α_o, is a measure of aerosol size distribution. A large α_o means that small particles dominate the aerosol population, while a small α_o means that large particles dominate. Ångström† states that a typical

† in 1961

value of α_o is 1.3. At Hampton Institute the daily average value of α_o ranges from 1.73 to - 1.39 and the monthly average data do not follow any consistent annual pattern. The equation used to calculate α_o is:

$$\alpha_o = 1.3 - 4.07 \log (\beta\text{-}875 / \beta\text{-}500),$$

where β-875 is the turbidity coefficient at 875 nm, and β-500 is the turbidity coefficient at 500 nm. From this equation it is apparent that α_o is determined by this beta ratio and that α_o is equal to 1.3 only when the β-875 / β-500 ratio is unity. Negative values of α_o are obtained when the beta ratio is greater than 2.087 which occurs when the local aerosol concentration measured at 875 nm is much greater than that measured at 500 nm.

C. Global/Direct and Diffuse/Direct Relationship with Atmospheric Turbidity

Monthly mean solar irradiance values listed in TABLE VII were used to calculate the average daily Global to Direct ratio for each month during 1982. The annual variation followed a pattern similar to that of the turbidity coefficient β_o. In Figure 12 both the Global to Direct ratio and turbidity coefficient β_o are plotted versus time of year using the 1982 data. When the local aerosol concentration increased, the direct solar irradiance contribution to global irradiance decreased and the Global to Direct ratio increased.

Under clear sky conditions, direct solar radiation in the earth's atmosphere is only affected by scattering and absorption due to aerosol particles and atmospheric gases such as water vapor and ozone. If the concentration of aerosols increases, the amount of radiation scattered out of the direct beam to form diffuse radiation also increases. The relationship between the Diffuse to Direct ratio and aerosol concentrations, indicated by the coefficient β_o, was investigated by plotting the average hourly diffuse to direct irradiance ratio and β_o versus time of day. On certain days, as illustrated for May 18, 1983 in Figure 13, the two parameters were nearly equal and followed a very similar variation throughout the day.

For the year 1982, 166 individual turbidity coefficient β_o measurements were plotted versus the diffuse to direct irradiance ratio calculated for the hour of each turbidity measurement. As shown in Figure 14 values of β_o varied by as much as a factor of two for a given Diffuse to Direct ratio value at the low end of the graph. A least squares linear regression was completed to obtain the relationship:

$$\beta_o = 0.5302 \left(DF / DR \right) + 0.074, \qquad \text{where,}$$

DF/DR is the ratio of the average hourly solar diffuse to direct solar irradiance values. The line represented by the equation above is also plotted on Figure 14. The correlation factor of 0.919 obtained indicated a close linear dependence between β_o and the average hourly diffuse to direct irradiance ratio inspite of the large variation discussed above.

Turbidity coefficient β_o data were plotted versus average ten-minute diffuse to direct irradiance data for each month. The linear regression analysis for each month resulted in a wide range of agreement with the assumed linear relationship. The November 1982 data set of five measurements was used to calculate a linear correlation of 0.989. However, the May 1983 data set of 44 measurements produced a correlation coefficient of only 0.062, implying that for this month a linear relationship between β_o and the diffuse to direct irradiance ratio does not exist. These results suggest that under the proper conditions the turbidity coefficient β_o is linearly related to the ratio of the diffuse solar irradiance to the direct solar irradiance, but do not identify the other important variables.

D. Correlations with Cloud Cover Fraction

An empirical model (NOAA, 1979) developed by the Air Resources Laboratory (ARL) of the National Oceanic and Atmospheric Administration was selected for correlation of the global solar irradiance data with cloud cover fractions. The two equations that relate global insolation to solar zenith angle and

opaque cloud cover fraction are:

$$SRC = A_0 + A_1 \cos ZA + A_2 \cos^2 ZA + A_3 \cos^3 ZA \quad (1)$$

and;

$$SR = SRC\,(B_0 + B_1\,OPQ + B_2\,OPQ^2 + B_3\,OPQ^3 + B_4\,RN). \quad (2)$$

SRC is the solar radiation hourly value for clear sky conditions. SR is the solar radiation hourly value for cloudy sky conditions. ZA is the zenith angle at the midpoint of each one-hour interval. OPQ is the average opaque cloud cover fraction. RN is a rain term that is equal to one if some form of precipitation is reported, otherwise it is zero.

The coefficients for clear sky conditions were calculated separately for mornings and for afternoons each month of the year in order to partially account for diurnal and seasonal variations in atmospheric turbidity, water vapor, and other such factors. The first and last partial hours of daylight were not included in the regression calculation. The coefficients for the second equation were calculated for mornings and afternoons combined using the data for the first full year of insolation measurements.

1. Clear Sky ARL Model Results

The clear sky data had to be analyzed before the cloudy sky data could be normalized by the expected clear sky values. Determination of clear sky hours was made using the Langley Air Force Base (LAFB) cloud cover observation data set. The number of totally clear sky hours was insufficient for meaningful determination of the coefficients of equation 1 for most months and, therefore, these data were supplemented with "nearly clear sky" data for which the strip chart trace showed no indication of clouds and for which the cloud cover fraction was less than two-tenths. These nearly clear sky data were selected from hours which were coded as clear at either the beginning or the end of the hour, or were coded as having low fractions of transparent, or semitransparent

clouds. These data were added in order to increase the number of points in the data set, and also to extend the meaningful range of the curve fit to zenith angles for which totally clear sky data were not available. This was consistent with the original use of the ARL model in the rehabilitation of SOLMET data.

The results of the application of this regression formula to our clear sky data are presented in TABLE IX for each month and in TABLE X for the first full year of global insolation measurements. The clear sky data are plotted in Figure 15 to show the extent of the agreement of the data with equation 1 for the one-year data set from March 1, 1981 through February 28, 1982. Most of the scatter in the data was caused by seasonal variations of the various atmospheric constituents. The individual regression coefficients for each month have relatively large probable statistical errors associated with them and cannot be compared easily with other coefficients for a different month or measurement site. The coefficient A_1 is the most accurate term and, for the one-year data set, it has only about a two percent probable error while even the algebraic sign of A_2 and A_3 is in doubt. The relative accuracy of the fit is demonstrated in the figure and, also, by comparison of the standard deviation to the data which gives a five to ten percent uncertainty in the midday insolation values.

2. Cloudy Sky ARL Model Results

The regression coefficients for clear sky mornings and for clear sky afternoons were used in equation 1 to determine the expected clear sky irradiance for each one-hour interval. The cloudy sky data were then normalized by the expected clear sky values and fit to equation 2 by using a nonlinear least-squares method. The cloud cover fractions were obtained from three different sources: 1) visual observations by trained observers (provided by the 3D Weather Squadron at nearby Langley Air Force Base-LAFB); 2) analysis of ground-based whole-sky photographs; and 3) analysis of GOES-EAST satellite photoprints.

Cloud cover fractions were calculated from the LAFB observations by averaging the value obtained five minutes before the hour began with the value at five minutes before the end of each hour (Eastern Standard Time). Hours with predominantly cirrus cloud cover were not used and thus only 2,926 one-hour averages were selected for use during the first one-year period. The data and curve plotted in Figure 16 are for dry conditions: RN=0. In order to satisfy computer space requirements, this large number of data was further reduced by the calculation of the mean value; the mean value plus, and minus, one standard deviation for each 0.05 step in cloud cover fraction from clear sky-0 to overcast sky-1 (21 steps plus overcast with precipitation times three values each for a total of 66 values). The results of the analysis of these LAFB derived fractions, which are presented in TABLE X and in Figure 16, reflect the use of these 66 values along with 26 values of partly cloudy skies with precipitation during the one-hour period.

The cloud cover fractions obtained from whole-sky photographs were plotted in Figure 17 for the one-year period. Most of the fractions were averages of the results of the analysis of two or three photographs and differ from the LAFB fractions in several respects. Only the first 70-75 degree field of view about the zenith in each photograph was used to measure cloud cover fraction as opposed to the standard 90 degree visual observation. Thin cloud cover and high clouds were not weighed heavily in the photographic analysis and thus this method provided a better measure of opaque cloud cover fraction. The curve obtained from the LAFB data is drawn in Figure 17 for comparison with the photograph derived fractions.

A number of cloud cover fractions were obtained by analysis of GOES-EAST, black and white, visual image, photoprints of the local area by using an overlay grid. The results are plotted in Figure 18 along with the LAFB curve. Photoprint derived fractions less than 0.25 appear to fit better than data from the other methods. Very small, low lying, clouds can dominate a ground-

based photo or visual observation, but may not be visible in the satellite photoprint because of the limited resolution. Very small thin clouds are unlikely to shade the pyranometer long enough to seriously affect the hourly insolation value. Thicker clouds with small transmittance and large reflectance can appear larger in the photoprint. This thickness effect shifts cloud cover fractions derived from photoprint analysis relative to ground-based fractions and improves the fit. All three plots show considerable deviations from the curve for individual points, but none of the points obtained from photographs or photoprints are significantly above the clear sky value in Figure 17 or 18, while several points in Figure 16 are over twenty percent above the expected clear sky value.

The partly cloudy hours with precipitation data provide an interesting test of the treatment of precipitation in equation 2. These data are plotted in Figure 19 with the overcast data represented by a mean value plus and minus one standard deviation. The lower curve represents the same coefficients as the other plots, but with RN=1. The upper curve uses the same coefficients but changes the precipitation term in equation 2 to $(B_4 \cdot OPQ \cdot RN)$ which guarantees no effect at OPQ = 0 (clear sky) and reduces to equation 2 for the normal overcast (OPQ = 1) precipitation condition.

IV. THEORETICAL-EMPIRICAL MODELING

The theoretical-empirical model developed by J. F. Foreman, was selected for use with our data and this method is presented below in detail. The clear sky part of this model was applied to a one-month, meteorological and radiometric data set as part of Mr. Foreman's proposed doctoral dissertation in Atmospheric Science at the University of Michigan. Our local data set was used to test and to develop fine details in the model for estimation of aerosol absorption. The month of February 1982 was selected as the test month for application of this model for the following reasons: (1) the ground albedo was expected to remain nearly constant throughout the month providing that there was no snow and that there was little change in the amount of ice in the tidal basin; (2) the automated data acquisition system provided short-time interval (one-minute) integrated data; and (3) clear sky conditions were sufficiently common to provide a data base for characterization of ground albedo and normal atmospheric absorption and scattering.

A. Summary of the Model

The method of estimation of global solar irradiance on a horizontal surface is an extension of the short-wavelength energy balance equation developed by Ellis and Vonder Haar (1978)

$$I_{hg} = \frac{1}{(1 - \alpha)} (I_o - I_r - I_a)$$ where:

I_{hg} is the horizontal global shortwave irradiance at the earth's surface;

α is the local ground albedo;

I_o is the horizontal extraterrestrial solar irradiance weighted by the spectral response of the satellite imaging device;

I_r is the total shortwave irradiance reflected to space by the earth's atmosphere and,

I_a equals the total (incident and reflected) shortwave radiation absorbed by the various components of the atmosphere.

The horizontal extraterrestrial insolation data were interpolated from measurements taken during the study period by an absolute cavity radiometer on board Nimbus 7 and reported by Hickey, et. al. (1982). The term I_r was calculated from the satellite measured brightness of the line elements and an appropriate bidirectional reflectance model for land and water surfaces developed by Raschke, et. al. (1973).

The portion of I_a due to absorption by water vapor was estimated using total precipitable water from nearby RAWINSONDE measurements of the vertical dewpoint distribution. The absorption of ozone and water vapor was calculated from parameterizations developed by Lacis and Hansen (1974). The absorption by permanent gases such as carbon dioxide and oxygen were calculated using a model presented by Burch, et. al. (1960) and by Yamamoto (1962).

The absorption of light by aerosols was computed as a residual from the measured four-minute global insolation data and the calculated absorption and reflection components. These calculated residuals were then parameterized to the column-mean relative humidity $\bar{f}$, as found from a RAWINSONDE sounding. The weighting was done using a mean vertical distribution of aerosols in the low levels selected from figure one of Shettle and Fenn (1975) according to the Ångström turbidity parameter, beta.

A fourth absorption portion of I_a is caused by clouds and was set to zero for this clear sky data set.

B. Data Sets

The meteorological data needed for this model were purchased from various sources. Most of the airways reports and weather data were purchased through

the Environmental Data Services, National Climatic Center, Asheville, North Carolina. The local study region is indicated in Figure 20 by the dotted lines and with the Hampton Institute measurement site indicated by an X. As noted in the legend, each meteorological site is represented by a separate number. The sources of data outside the study region were used to establish parameters at the boundaries of the study region and as back-up data sets since several data sources did not report hourly. A summary of the data sets used in the analysis is given below in outline form.

1. Satellite Data

   a. Source: GOES-East visible and infrared digitized brightness values.

   b. Resolution: 0.9 km x 0.9 km visible, 3.7 km x 3.7 km infrared (at nadir).

   c. Data Array Coordinates:

Point	Satellite (Nominal) line x element	Geographical latitude x longitude
Center -	2990 x 7490	37.019^{O}N x 76.338^{O}W
NW Corner -	2949 x 7451	37.587^{O}N x 76.884^{O}W
NE Corner -	2949 x 7532	37.584^{O}N x 75.801^{O}W
SE Corner -	3040 x 7532	36.470^{O}N x 75.798^{O}W
SW Corner -	3040 x 7451	36.473^{O}N x 76.858^{O}W

   d. Period: Clear Sky Hours for February 7, 8, 11, 13, 15, 20, 22, 23, 25 and 28, 1982; Cloudy Sky Hours for February 4, 13, 17, 18, 21 and 24, 1982;

2. Meteorological

   a. Insolation:

      i. Type: horizontal global - 0.3 μm to 2.8 μm.

      ii. Frequency: ten-minute totals centered on satellite scan time (GMT).

      iii. Source: Eppley PSP one-minute integrated data at Hampton Institute.

   b. Humidity

      i. Hourly surface airways reports of temperature, dew point, and altimeter settings from local airport, Coast Guard, Air Force, Navy, and Army weather data sources for low level data.

ii. Radiosonde data from Wallops Island, Sterling Virginia, Cape Hatteras and Greensboro, North Carolina for upper level data.

c. Cloud Parameters (not used in the clear sky analyses)

i. Cloud fraction: Hampton Institute photographs and satellite brightness readings.

ii. Cloud type and height: Langley Air Force Base observations.

iii. Water content: radar reports (facsimile charts) from local airports.

iv. Cloud top temperature: Infrared satellite data.

d. Ozone and Aerosols

i. Turbidity readings at Hampton Institute (or from a network of stations east of the Mississippi River, including Raleigh-Durham, North Carolina, for those cases when turbidity readings were not taken at Hampton Institute).

ii. Dobson spectrophotometer readings of total ozone column over Nashville, Tennessee, Tallahassee, Florida, Wallops Island, Virginia, and Washington, D.C. obtained from the World Ozone Data Center, Environment Canada, Toronto, Canada.

3. Miscellaneous

a. Ground albedo: calculated from clear sky satellite brightness values using an equation developed by Vonder Haar and Ellis (1975).

b. Elevation: most points within the study region are treated as being at sea level but use of United States Geological Survey Maps was made to ascertain elevations throughout the study region.

C. Results

A computer program "ABSOR.BAS", which solves the energy balance equation to estimate the absorption of wide-band short-wave radiation (hereafter called solar radiation) by aerosols was run for the Hampton Institute Solar Measurement Site (hereafter called SMS). The results for each case, including all of the terms in the energy balance equation, are presented in Table XI. The fractional absorption (the absorption by aerosols, estimated from energy balance, and divided by the incident solar flux beneath the ozone layer), as well as the parameters used in each least-squares fit, are presented in Table XII for each case. These results are also presented in Figures 21 through 23, where variables not explicitly named are assigned their mean values.

One very salient feature of the absorptions by aerosols in both of the tables is that these are predominantly negative in value. This indicates a systematic overestimation of one or more of the terms of the energy balance equation; possibly the measured horizontal global insolation term (more on this later) or the gaseous absorption term, but most likely in the upwelling reflection term owing to defects in the bi-directional reflectance model and in the image calibration. For this reason, the relative sun-satellite azimuth, Kasten's (1966) relative optical air mass (hereafter called ROAM, which is directly associated with the solar zenith angle) and the hours after 0000 GMT, January 1, 1982 were included in the least-squares-fit analyses. The sun-satellite azimuth and the ROAM were included to account for shortcomings in the bi-directional reflectance model and the hours parameter was included to account for time-related "drifts" in the calibrations of the eight visual channels.

Two of the tabulated cases were not used in any of the statistical analyses. Case No. 2 was omitted because of the presence of clouds

covering part of the 101 line x 101 element display sector allegedly containing the Hampton Institute SMS. Because of the high reflectivity of these clouds, the contrast of the non-cloudy portion of this sector was greatly reduced (the contrast of this display is made by dividing the range of brightness in the displayed sector into eight equal intervals and assigning a symbol to each interval) making the act of locating Hampton Institute very difficult and uncertain. Case No. 14 was omitted because, owing to the late hour of this image, the solar zenith angle was very large requiring an unreasonable extrapolation of the bi-directional reflectance model. Also, because of the late hour, the visual image was very dark causing great difficulty in locating Hampton Institute.

A third case, No. 19, however, could not be omitted on any such physical grounds, even though the fractional absorption for this case is lower than any of the others and much lower than any least-squares-fit formula prediction on this case. In fact, the inclusion or omission of this particular point made a great difference in the very nature and course of the least-squares-fit analysis and in the formula found from such an analysis. As a result, two sets of analyses, with and without case No. 19, were made.

1. Case No. 19 included (two excluded cases):

   i. For turbidity related parameters excluded*:

$$i_{AA}^{ii(-2)} = 0.0932254 - 0.000573405\ \theta_{ss} - 0.0635565\ \bar{f}$$

   where i_{AA} = fractional absorption by atmospheric aerosols;

   ii(-2) = two independent parameters with two cases excluded;

   θ_{ss} = relative sun-satellite azimuth (degrees) using the convention of Raschke et al. (1973) which defines

*This was done to create a predictive formula which could be used in those large regions of the Earth's surface far from any Volz Sunphotometer observation sites.

this angle as the horizontal projection of the deflection of a photon from its incident direction (or the absolute value of 180 degrees minus the difference between the solar and viewing azimuths) rather than the absolute value of the simple difference between the solar and viewing azimuths; and,

$\bar{f}$ = the mean relative humidity and is included as a "non-turbidity related parameter" since it can still be estimated without β, albeit less accurately, by weighing with a mean (β-independent) aerosol profile.

The least squares fit analysis produced a multiple correlation coefficient, R = 0.44145 and an adjusted multiple correlation coefficient, R' = 0.324865.

ii. For turbidity-related parameters included, the parameterization depends on the minimum acceptable value of p ($=P[F \leq F_p]$ (Ostle, 1963; Bevington, 1969) chosen in finding the F-statistic:

a. If p is chosen to be $\geq$ 68%, only one parameter qualifies as an acceptable predictor and the result is:

$$i_{AA}^{i(-2)} = -0.0544005 + 0.138264\ \tau_{45}$$

where i(-2) = one independent parameter with two cases included and,

τ_{45} = aerosol optical depth at λ = 0.45 μm.

$$\tau_{45} = m_{kp}\ (0.45)^{-\alpha},$$

where $m_{kp} = m_k\ p'/po$,

m_k = Kasten's (1966) ROAM,

p' = atmospheric surface pressure (kPa) at the point of interest (in this case, the Hampton Institute SMS),

p_o = 101.325 kPa (= 1013.25 mb),

and

β and α = Volz-Ångstrom turbidity coefficient and exponent, respectively.

The analysis produced a multiple correlation coefficient, R = 0.541201 and an adjusted multiple correlation coefficient = 0.50565;

b. If, however, p = 67%, almost all of the analysed predictors become valid in a stepwise least-squares process. In fact, the number of predictors used was limited to seven, not because of the computed F-statistic for predictors beyond the seventh, but because seven is the maximum number of independent variables which the multiple regression program ("COSAF" statistical package) could handle:

$$i_{AA}^{vii(-2)} = -0.065407 + 0.367642\ \tau_{45} - 0.000443137\ \theta_{ss} - 0.0325417\ m_{kp}\beta(\lambda_{max}(\alpha))^{-\alpha} + 0.00863353\ m_{kp} - 0.157439\ \bar{f} + (9.87231 \times 10^{-5})\ H - 0.00381737\ \alpha$$

where

$\lambda_{max}(\alpha)$ = wavelength of maximum aerosol attenuation of solar radiation found by setting the partial derivative with respect to λ of the product of the Planck function and $\beta\lambda^{-\alpha}$, equal to zero. After eliminating the zero and infinite roots, the resulting equation:

$$\exp(c'/\lambda) = (\alpha + 5)\,\lambda/((\alpha + 5)\lambda - c')$$

where

$c' = hc/kT = 2.48067\ \mu m$,

h = Planck constant = 6.6256×10^{-27} erg s,

c = speed of light <u>in vacuo</u> = 2.99725×10^{10} cm/s,

k = Boltzmann constant = 1.38054×10^{-16} erg/K, and

T = mean effective solar radiative temperature = 5800 K (Glasstone, 1965), was numerically solved for λ as a function of α (very tricky, as there is a very sharp $-\infty$ to $+\infty$ singularity very close to the solution, especially at the larger values of α). This function is approximated to within 0.3% by:

$$\lambda_{max}(\alpha) = 0.0864642 - 0.00622149\alpha + 1.75525/(\alpha + 4.25)$$

and

H = Hours since 0000 GMT, January 1, 1982.

The analysis produced a multiple correlation coefficient, $R = 0.825926$ and an adjusted multiple correlation coefficient, $R' = 0.71492$.

2. Case No. 19 excluded (total of three excluded cases):

   i. For turbidity-related parameters excluded:

   $$i_{AA}^{ii(-3)} = 0.132772 - 0.000797235\ \theta_{ss} - (2.41835 \times 10^{-5})H$$

   multiple correlation coefficient, $R = 0.642801$ and an adjusted multiple correlation coefficient, $R' = 0.586281$.

   ii. For turbidity-related parameters included:

   $$i_{AA}^{iii(-3)} = 0.0485699 - 0.000488838\ \theta_{ss} + 0.0229239\ \alpha - 0.00646946\ \alpha^2$$

   The results were a multiple correlation coefficient, $R = 0.84393$ and an adjusted multiple correlation coefficient, $R' = 0.811331$.

The results of all these least-squares fits are presented in Figures 24 through 28.

One rather surprising feature of all of these results is that wherever $\bar{f}$ appears, it has a negative coefficient whereas one would expect the opposite (e.g. Mészarós, 1971; Hänel, 1972, 1976; Covert et al., 1972; Nair and Vorha, 1975; Fitzgerald, 1975; Fitzgerald et al., 1982). One possible

explanation of this is that there is a systematic overestimation of the absorption of solar radiation by water vapor, since the radiatively effective water vapor column on which the water vapor absorption estimation is based is strongly associated with $\bar{f}$. Three possible sources of this are:

1. The program "WATAIR.BAS" that estimates the radiatively effective water vapor column, w, from a sounding;
2. The program "OZONAL.BAS" which fits a function of the form:

   $$z = c_1 + c_2 L + c_3 E + c_4 LE$$

   where z is the quantity being fitted, L is the negative of the line number, E is the element number and $c_1, \ldots, c_4$ are coefficients determined from the input data, using water vapor column observations from four upper-level stations just outside the study region. This function was used to obtain the radiatively effective water vapor column over Hampton Institute given Hampton Institute's line and element numbers in nominal GOES-east coordinates; and
3. In the formula of Lacis and Hansen (1974) which estimated the absorption of solar radiation by water vapor given the local radiatively effective water vapor column and the relative optical air mass.

One predictor which was applied to this analysis, but without success, was the formula modified from Hoyt (1978,1979) which purported to estimate the absorption of solar energy by aerosols:

$$i''_{AA} = (1 - \omega_s)(1 - g(\beta)^{m_{kp}})$$

where

ω_s = albedo of single scattering by aerosols = 0.95 and

$g(\beta) = 0.937 - 1.044\ \beta + 0.00575/(\beta + 0.108)$ (which gives an acceptable fit to the tabulations of $g(\beta)$ by Hoyt (1978,1979)).

It is not known why this formula fared so poorly as a predictor of the absorption of solar radiation by aerosols. It may well be that the fault

lies with the modification of Hoyt's formula which was originally $i'_{AA} = (1 - \omega_s)\, g(\beta)^{m_{kp}}$. Numerous attempts since last October to contact Mr. Hoyt for guidance on this matter have failed. Alternatively, this failure may be from errors in the estimation of absorption by aerosols from energy balance.

V. SUMMARY AND CONCLUSIONS

Energy balance is a superb, fundamentally sound method, both for estimating the insolation at the Earth's surface and for investigating residual effects, such as the absorption of light by clouds or aerosols and errors resulting from defects in the bi-directional reflectance models and in the calibration of the imaging device. In the case of this study, energy balance was used to investigate the absorption of solar radiation by aerosols and defects in the bi-directional reflectance model (Raschke et al., 1973) and in the calibration of the eight visual channels of the GOES-east satellite (Norton et al., 1980).

The results of this study are somewhat equivocal since they are excessively sensitive to the inclusion or exclusion of a single case (No. 19). Obviously, a much larger data base is needed before some decisive conclusions may be reached, even for one location and during one month.

Some facts about the results, however, are not so equivocal. For one thing, there is a decided negative dependence of the fractional absorption by aerosols on the relative sun-satellite relative azimuth angle, θ_{ss}, with or without case No. 19. The coefficient on θ_{ss} is small in magnitude because θ_{ss} was given in degrees in this study. This strong dependence on θ_{ss} indicates a systematic error in the bi-directional reflectance model used in this study. This is also indicated by the dependence on the pressure-correlated relative optical air mass, m_{kp} (directly associated with the solar zenith angle), in the predictive formula for p = 67% with case No. 19 and turbidity-related parameters included. The dependence on the viewing zenith angle was not investigated in this study because of a limitation inherent in any view of a single Earth-surface point from a single geostationary satellite; namely, the viewing zenith angle varies very little, if at all. In fact, in this study, the range of this angle was less than two degrees.

Other strong dependencies found in this study were on the computed optical depth at $\lambda = 0.45$ /um and on the Volz-Ångström turbidity exponent, α, especially on the square of α, in the predictive formulae including turbidity-related parameters.

Other, weaker dependencies were found on: the aerosol profile (selected by β) weighted column mean relative humidity, $\bar{f}$; the aerosol optical depth at the α-dependent wavelength of maximum absorption, $m_{kp}^{\beta} (\lambda_{max}(\alpha))^{-\alpha}$; and the number of hours, H, since 0000 GMT, January 1, 1982 which indicates a time dependence in the response (hence, in the calibration) of the satellite's visual channels. However, only a very weak dependence was found on a modification of the Hoyt (1978,1979) prediction, $(1 - \omega_s)(1 - g(\beta)^{m_{kp}})$. This parameter will, however, be retained as a regressive parameter to be investigated in future studies on a different or expanded data base.

It has also been found that there may be a large uncertainty, as much as 30%, in the estimation of the radiation reflected spaceward by the Earth-atmosphere system. Of this, 20% may be due to problems in the calibration of the digitised visual images from geostationary satellites (Muench, 1981; how this figure of 20% was arrived at will be discussed in Appendix IV.) The remaining approximate 20% (in a pythagorian sum) is an educated guess on the uncertainty inherent in a bi-directional reflectance model and is comparable to the standard deviations which Davis and Cox (1981) found in their own bi-directional reflectance model.

Another uncertainty arises from using four-minute totals from an integrator to obtain the measured mean horizontal global insolation at the Earth's surface. An integrator yields acceptable accuracy for totals of thirty minutes or more, but for shorter period totals, a different type of digitising device, or even an average of point measurements from the

analog trace, should be used, especially under low levels of daylight illumination (e.g., under cloud cover or near sunrise or sunset). This stands as a recommendation for future research as short-period averages are necessary in a high-resolution (in this case, the A-scale or 0.9km x 0.9 km, the highest nadir-point resolution available from an SMS/GOES satellite) study to ensure that cloud cover or illumination conditions do not appreciably change during the measurement.

Another recommendation regards the bi-directional reflectance model. The model of Raschke et al. (1973) was chosen only because it was "tried and true", having been in the literature for a long time and used by numerous investigators in solar radiation and Earth radiation budget studies. The only other extensive model that was available at that time, Davis and Cox (1981), was rejected because the "bugeye" device used in that study sampled at only three nadir viewing angles (0^{o}, 30^{o} and 60^{o}) whereas the nadir viewing angle in this study never strayed from the 40^{o} - 43^{o} range. Another model (Stowe et al., 1980) has been brought to our attention which may be superior to either previously identified model.

Ideally, one should hire an aircraft and, using a photometric device as similar as possible in its spectral characteristics to that in the SMS/GOES VISSR, to make one's own survey of the angular (bi-directional) reflectance of the solar measurement site under as wide and as complete a range of solar zenith angles as possible during the study period. A further refinement would be to account for the angular reflectance of the overlying cloud-free atmosphere, including the changes of this angular reflectance with aerosol loading (e.g., Braslau and Dave, 1973). Both of these refinements would greatly improve the accuracy and reliability of the estimates of the solar radiation reflected spaceward by the Earth-atmosphere system. However, one considerable obstacle remains to complete

accuracy in this estimation; the calibration of all eight GMS/GOES VISSR visual channels. Although numerous investigators (e.g., Bauer and Lienesch, 1975; Hinton, Appendix 1 in Norton et al., 1980; Muench, 1981) have been working on this very thorny problem, none have yet found a true solution.

Another recommendation would be to use a solar measurement site as close as possible to a location where turbidity, upper level RAWINSONDE and surface pressure (even Dobson spectrophotometer ozone) observations are made, thereby minimizing errors arising from extrapolating values of meteorological variables in space to the solar measurement site. Also, if the investigator has any control over such matters, the turbidity measurements should be made as close as possible in time to the expected satellite scan time (the time at which the VISSR on board the spinning satellite actually scans the measurement site as opposed to the nominal or actual image start time), thereby minimizing errors due to time extrapolation. Such extrapolations, both in time and space, can produce appreciable errors in the turbidity parameters, especially in an inhomogeneous atmosphere.

A more complete study of the errors and their propagation in the computations in this study will be made by Mr. Foreman in his Ph.D. thesis at the University of Michigan. This thesis is now in preparation.

LIST OF TABLES

TABLE I

HAMPTON INSTITUTE SOLAR ENERGY MEASUREMENT SUMMARY

Measurement	Instrumentation	Data Frequency	Start	End
SOLAR IRRADIANCES				
Global	Eppley PSP with WG7 clear glass dome	One-hour integrated and continuous chart	Feb. 17, 1981	-
		One-minute integrated*	Feb. 1, 1982	Jul. 31, 1983
Direct	Eppley NIP with quartz glass and solar tracker	One-hour integrated and continuous chart	Oct. 1, 1981	-
		One-minute integrated*	Feb. 1, 1982	Jul. 31, 1983
Diffuse	Eppley PSP with WG7 clear glass dome	One-hour integrated and continuous chart	Oct. 1, 1981	-
		One-minute integrated*	Mar. 1, 1982	July 31, 1983
ATMOSPHERIC EMITTANCE	Eppley PIR	One-hour integrated and continuous chart	Mar. 18, 1981	-
		One-minute integrated*	Mar. 1, 1982	Jul. 31, 1983
ATMOSPHERIC PROPERTIES				
Aerosol Extinction @ 380 and 875 nm Turbidity @ 500 nm Precipitable Water	Volz Sunphotometer	Approximately one hour intervals for clear sky	Mar. 24, 1981	-

*After March 13, 1982 the computer automated radiometric data sampling rate was set at one-minute from 0400 EST to 2000 EST and at ten-minutes from 2000 EST to 0400 EST.

TABLE II

RADIOMETRIC INSTRUMENTATION WAVELENGTH CHARACTERISTICS

Instrument	Normal Observation Wavelength Range
Eppley Precision Spectral Pyranometer	0.285 to 2.8 microns
Eppley Precision Infrared Radiometer	4.0 to 50.0 microns
Eppley Normal Incidence Pyrheliometer	0.285 to 4.5 microns
Eppley Hickey-Frieden Absolute Cavity Pyrheliometer	0.2 to 50 microns
Additional Wavelength Ranges for the Pyranometers and Pyrheliometers	0.53 to 2.8 microns
	0.63 to 2.8 microns
	0.70 to 2.8 microns
Volz Sunphotometer	Center of Band - Halfwidth
	380 nm - 11 nm
	500 nm - 40 nm
	875 nm - 17 nm
	940 nm - 16 nm

TABLE III RADIOMETER CALIBRATION SUMMARY

Radiometer	Calibration Information			Sensitivity Factor ($\mu V m^2 w^{-1}$)
	Date	Comparison With:	Performed By:	
Precision Spectral Pyranometer				
Eppley PSP #20022F3	10/1/80	Standard References	Eppley Laboratory	10.55
	4/30/81	PSP # 20613F3	Hampton Institute	*
	6/24/81	PSP # 20613F3	Hampton Institute	*
	6/21/82	PSP # 20613F3	Hampton Institute	*
	7/8/82	Standard References	Eppley Laboratory	10.00†
	9/6/82	PSP # 20613F3	Hampton Institute	*
	7/7/83	PSP # 22046F3	Hampton Institute	*
	7/18/83	Standard References	Eppley Laboratory	9.82
Eppley PSP # 20613F3	2/28/81	Standard References	Eppley Laboratory	11.10
	7/15/82	PSP # 20022F3	Hampton Institute	10.62†
	8/19/82	Standard References	Eppley Laboratory	10.67
	7/7/83	PSP # 22046F3	Hampton Institute	*
		Standard References	Eppley Laboratory	
	9/9/83	Standard References	Eppley Laboratory	10.52
Eppley PSP # 22046F3	10/13/82	Standard References	Eppley Laboratory	10.47
Normal Incidence Pyrheliometer				
Eppley NIP # 20254E6	3/4/81	Standard References	Eppley Laboratory	9.21
	5/12/82	H-F Pyrheliometer	Hampton Institute	**
	5/5/83	H-F Pyrheliometer	Hampton Institute	**
Precision Infrared Radiometer				
Eppley PIR # 20078F3	10/6/80	Standard References	Eppley Laboratory	4.95
	7/7/82	Standard References	Eppley Laboratory	4.86
	8/1/83	Standard References	Eppley Laboratory	4.90

* These sensitivity factors are unchanged within the ± 2% accuracy of the instruments.
** The sensitivity factor was unchanged within the accuracy of the calibration instruments (1.5%).
† Eppley Laboratory changed calibration standards October 1981 by 2.6%.

TABLE IV RADIOMETRIC DATA CORRECTION FACTORS

Month	Year	Global Irradiance	Direct Irradiance	Diffuse Radiance	Atmospheric Emittance
March	1981	1.033	1.000	-	-
April	"	1.034	"	-	1.0012
May	"	1.035	"	-	1.0024
June	"	1.036	"	-	1.0036
July	"	1.029	"	-	1.0049
August	"	1.030	"	-	1.0061
September	"	1.031	"	-	1.0073
October	"	1.031	"	1.0413	1.0085
November	"	1.032	"	1.0426	1.0098
December	"	1.033	"	1.0439	1.0110
January	1982	1.034	"	1.0452	1.0123
February	"	1.034	"	1.0464	1.0135
March	"	1.035	"	1.0475	1.0148
April	"	1.036	"	1.0488	1.0160
May	"	1.036	"	1.0499	1.0173
June	"	1.037	"	1.0510	1.0185
July	"	1.038	"	1.0550	1.0185
August	"	1.057	"	-	1.0178
September	"	1.040	"	1.0582	1.0170
October	"	1.043	"	1.0598	1.0162
November	"	1.045	"	1.0614	1.0155
December	"	1.048	"	1.0630	1.0147
January	1983	1.051	"	1.0646	1.0140
February	"	1.013	"	1.0106	0.9948
March	"	1.015	"	1.0121	0.9940
April	"	1.018	"	1.0137	0.9933
May	"	1.020	"	1.0152	0.9926
June	"	1.023	"	1.0168	0.9918
July	"	1.025	"	0.9551*	1.0183

*Required for one-minute integrated data only for July 1983.

TABLE V

DATA RECOVERY RECORD: HOURLY INTEGRATED IRRADIANCES

Year	Month	Number of Hour-Values Stored on Magnetic Tape			
		Global Solar	Direct Solar	Diffuse Solar	Atmospheric Emitted
1981					
	February	300	-	-	120
	March	744	-	-	664
	April	720	-	-	718
	May	744	-	-	744
	June	719	-	37	720
	July	741	-	117	741
	August	740	-	0	741
	September	720	13	43	720
	October	743	529	712	742
	November	720	615	716	720
	December	742	611	732	740
1982					
	January	744	676	639	722
	February	672	668	672	672
	March	743	738	744	658
	April	720	692	716	720
	May	740	715	721	744
	June	720	720	479	512
	July	744	744	279	406
	August	741	741	198	742
	September	720	720	567	720
	October	742	742	744	744
	November	720	719	720	720
	December	744	740	744	744
1983					
	January	742	742	738	693
	February	670	671	667	665
	March	744	711	742	744
	April	744	699	729	744
	May	744	734	744	744
	June	720	690	718	711
	July	744	650	744	249

TABLE VI DATA RECOVERY RECORD FOR AUTOMATED DATA ACQUISITION SYSTEM
ONE AND TEN MINUTE INTEGRATED IRRADIANCES

Month-Insolation Component	Maximum Possible Number of Data Records	Amount Recovered by Computer Number - Percent	Number of Missing Data Records			
			User Interrupt	System Crash	System Calibration	Other
February - 1982						
Global*	40,320	36,326 - 90.1	2,205	1,190	-	599
Direct*	"	35,163 - 87.2	3,358	1,200	-	599
March						
Global	36,648	35,369 - 96.5	446	678	-	155
Direct	"	35,381 - 96.5	433	679	-	155
Diffuse**	"	34,434 - 94.0	263	679	-	1,272
Infrared**	"	26,470 - 72.2	257	679	-	9,242
April						
Global	30,240	29,673 - 98.1	61	407	-	99
Direct	"	29,708 - 98.2	26	407	-	99
Diffuse	"	29,708 - 98.2	26	407	-	99
Infrared	"	29,708 - 98.2	26	407	-	99
May						
Global	31,248	29,519 - 94.5	17	1,712	-	-
Direct	"	29,519 - 94.5	17	1,712	-	-
Diffuse	"	29,519 - 94.5	17	1,712	-	-
Infrared	"	29,519 - 94.5	17	1,712	-	-
June						
Global	30,240	28,232 - 93.4	181	1,827	-	-
Direct	"	28,232 - 93.4	181	1,827	-	-
Diffuse	"	16,112 - 53.3	181	1,827	12,120	-
Infrared	"	19,453 - 64.3	181	1,827	8,779	-

*One-minute readings only from 0942 February 1, 1982 to 2000 EST March 13, 1982 and ten-minute readings at night after March 13.

**One-minute readings only from 2038 EST March 1, 1982 to 2000 EST March 13, 1982 and ten-minute readings at night after March 13.

TABLE VII AVERAGE DAILY TOTAL IRRADIANCE SUMMARY

Month	Year	Global Irradiance (kJm^{-2})	Diffuse Irradiance (kJm^{-2})	Direct Irradiance (kJm^{-2})	Atmospheric Emittance (kJm^{-2})
March	1981	15,610	-	-	19,242
April	"	19,814	-	-	30,773
May	"	19,919	-	-	32,425
June	"	22,604	-	-	37,285
July	"	21,971	-	-	37,746
August	"	18,457	-	-	35,701
September	"	18,378	-	-	33,264
October	"	12,852	5,155	-	30,114
November	"	9,292	3,838	-	27,288
December	"	6,426	2,808	-	25,567
AVERAGE -	1981	16,532	-	-	30,940
January	1982	7,697	3,899	10,552	24,379
February	"	9,965	4,637	10,634	26,600
March	"	14,188	5,911	13,219	26,896
April	"	19,174	7,110	15,095	28,458
May	"	22,997	10,105	17,708	33,757
June	"	21,301	11,225	12,848	36,169
July	"	21,629	-	14,087	-
August	"	19,199	-	13,450	32,742
September	"	15,966	7,798	12,866	31,086
October	"	11,635	5,508	12,013	28,087
November	"	8,831	4,396	10,300	26,532
December	"	6,131	3,222	7,538	25,286
AVERAGE -	1982	14,893	6,381	12,526	29,090
January	1983	8,017	3,783	9,990	22,961
February	"	10,539	4,828	10,958	22,945
March	"	13,150	6,190	10,163	25,954
April	"	17,605	8,051	12,254	26,902
May	"	22,624	10,083	16,330	27,515
June	"	24,421	10,787	17,395	31,648
July	"	25,027	10,577	19,681	33,880

TABLE VIII

AVERAGE ATMOSPHERIC AEROSOL EXTINCTION AND TURBIDITY PARAMETERS

Month/Year	# of Days	Aerosol Extinction Parameter – Tau 380 nm	500 nm	875 nm	Turbidity Parameters $\beta\phi$	$\alpha\phi$
Feb 1981	3	0.527	0.127	0.073	0.064	1.004
Mar	8	0.353	0.172	0.856	0.073	1.176
Apr	6	0.378	0.172	0.114	0.105	0.576
May	3	0.455	0.217	0.144	0.131	0.643
June	5	0.914	0.547	0.262	0.220	1.30
July	7	0.871	0.653	0.353	0.306	0.942
Aug	7	1.055	0.667	0.307	0.256	1.264
Sept	10	0.612	0.345	0.173	0.151	0.688
Oct	3	0.304	0.107	0.108	0.109	–0.004
Nov	2	0.284	0.105	0.088	0.085	0.291
Dec	2	0.273	0.129	0.067	0.058	1.156
Jan 1982	5	0.356	0.146	0.103	0.096	0.507
Feb	1	0.327	0.081	0.105	0.112	–0.490
Mar	7	0.477	0.182	0.146	0.139	0.379
Apr	4	0.332	0.123	0.133	0.137	–0.252
May	2	0.635	0.254	0.234	0.230	0.045
June	6	0.940	0.511	0.323	0.298	0.596
July	5	1.475	0.925	0.481	0.414	0.932
Aug	9	1.402	0.893	0.482	0.417	0.943
Sept	2	0.654	0.253	0.158	0.141	0.829
Oct	4	0.420	0.171	0.140	0.135	0.304
Nov	2	0.625	0.295	0.198	0.182	0.523
Dec	2	0.446	0.235	0.174	0.162	0.543
Jan 1983	5	0.403	0.194	0.172	0.167	0.194
Feb	4	0.556	0.292	0.214	0.199	0.508
Mar	2	0.550	0.233	0.217	0.214	0.093
Apr	2	0.670	0.313	0.270	0.261	0.244
May	7	0.643	0.151	0.230	0.258	–0.868
June	4	1.021	0.436	0.318	0.298	0.408

TABLE IX ARL REGRESSION COEFFICIENTS FOR CLEAR SKY GLOBAL SOLAR IRRADIANCE

Time of Day - Month	Number of Hours		Regression Coefficients (kJ m^{-2})			
	Clear Only	Nearly Clear	A_0	A_1	A_2	A_3
Mornings						
March, 1981	10	0	- 212	3366	1256	- 648
April	8	11	- 104	2729	2081	- 961
May	9	23	43	1422	3992	-1919
June	5	8	- 101	2174	1141	360
July	6	5	- 94	2423	1022	144
August	20	5	- 428	4784	-4068	3337
September	35	5	- 86	2268	2797	-1523
October	9	0	- 400	5609	-5652	5508
November	10	10	- 544	2830	1811	- 482
December	1	18	- 176	3791	18	871
January, 1982	11	1	22	1735	6966	-6289
February	1	6	- 144	3424	1102	- 70
Afternoons						
March, 1981	14	0	- 187	3856	- 839	1130
April	5	12	- 50	2419	2740	-1364
May	0	12	173	598	6638	-3834
June	5	2	- 7	1184	5407	-3143
July	0	6	- 86	1699	3161	-1206
August	4	2	61	652	5238	-3351
September	17	4	54	756	5738	-2880
October	1	8	- 32	1735	6185	-5404
November	8	2	- 270	3949	191	148
December	5	4	- 486	6163	-6674	7348
January, 1982	12	2	54	936	8766	-8973
February	1	8	- 11	2160	3766	-1897

TABLE X

ARL COEFFICIENTS FOR THE FIRST YEAR DATA SET
(March 1, 1981 through February 28, 1982)

Clear Sky Global (Fit to Equation 1)	No. of Points	Regression Coefficients (kJ m^{-2}) A_0	A_1	A_2	A_3	Standard Deviation (in kJ m^{-2})
Mornings						
Clear Sky Only	125	-140	3049	1138	- 616	162
Clear & Nearly Clear	217	-209	3708	- 302	310	158
Afternoons						
Clear Sky Only	72	-252	3920	- 454	554	133
Clear & Nearly Clear	135	-130	2754	2336	-1328	122

Cloudy Sky Global (Fit to Equation 2)	No. of Points	Regression Coefficients B_0	B_1	B_2	B_3	B_4	Standard Deviation
Reduced LAFB Data Set	92	1.004	-0.353	0.789	-1.089	-0.215	0.14
Satellite Photoprints	62	1.017	-0.468	-0.182	0.033	-0.253	0.13
Whole-Sky Photographs	104	0.955	-0.615	0.975	-0.850	-0.319	0.14

TABLE XI PARAMETERIZATION INPUT SUMMARY

Case No.	Date (Feb. 1982)	Time (GMT)	Surface Insolation (Wh/m^2)	Extraterrestrial Horizontal Insolation (Wh/m^2)	Upwelled Reflectance (Wh/m^2)	Aerosol Absorption (Wh/m^2)	Gaseous Absorption (Wh/m^2)
4	7	1407	356.7	501.3	91.19	3.12	81.24
5	7	1607	620.4	805.9	155.19	-22.47	106.54
6	7	1807	635.9	833.4	153.92	-9.09	107.86
7	7	2007	418.8	575.8	108.95	-1.71	86.17
9	8	1406	325.7	502.9	113.73	0.74	90.99
10	8	1606	604.9	810.0	152.18	-18.04	123.43
11	8	1806	604.9	840.2	156.36	4.42	127.06
13	11	2006	416.8	603.3	124.84	-7.83	103.86
15	13	2207	82.0	140.8	45.64	-0.78	140.77
17	14	1606	604.9	847.9	157.12	-4.34	142.72
19	20	1406	403.3	569.4	149.64	-49.19	100.65
23	23	1406	403.3	582.4	116.00	-7.94	106.13
24	23	1606	666.9	897.5	163.74	-15.45	140.17
25	25	1506	604.9	783.0	139.61	-25.16	116.16
26	25	1637	760.0	946.9	176.56	-52.94	129.25
27	25	1706	775.5	963.8	202.34	-74.62	127.93
28	25	1807	744.5	943.6	168.44	-29.19	124.48
29	25	1907	651.4	849.6	145.20	-5.36	114.92
30	28	1807	729.0	960.3	164.51	-14.70	144.79
31	28	2007	496.3	702.9	133.16	0.61	115.94
32	28	2207	108.6	225.5	62.04	8.62	85.66

TABLE XII PARAMETERIZATION OUTPUT AND RESULTS

Case No.	Fractional Absorption by Aerosols	Kasten's Relative Air Mass	Optical Depth τ (0.45/μm)	Hoyt's Prediction	Relative Sun Satellite Azimuth (^{o})	Turbidity Alpha	Turbidity Beta	Average Relative Humidity
4	0.00647	2.850	0.3760	0.01067	131.8	2.309	0.0595	0.299
5	-0.02872	1.781	0.3616	0.00676	161.3	2.303	0.0575	0.282
6	-0.01123	1.719	0.3177	0.00622	168.2	2.210	0.0544	0.270
7	-0.00307	2.477	0.2029	0.00882	141.7	1.631	0.0552	0.263
9	0.00154	2.830	0.3326	0.01001	131.4	2.240	0.0556	0.331
10	-0.02294	1.765	0.3334	0.00652	160.8	2.239	0.0558	0.318
11	0.00542	1.699	0.3334	0.00631	167.6	2.236	0.0559	0.308
13	-0.01346	2.354	0.3553	0.01486	142.0	1.491	0.1080	0.506
15	-0.00611	9.266	0.3696	0.03686	116.3	1.590	0.1039	0.302
17	-0.00526	1.675	0.3819	0.01041	158.8	1.675	0.1003	0.503
19	-0.08997	2.457	0.2326	0.00457	129.2	2.708	0.0268	0.521
23	-0.01422	2.414	0.3063	0.00581	128.2	2.750	0.0341	0.506
24	-0.01778	1.571	0.3095	0.00356	156.4	2.823	0.0325	0.481
25	-0.03312	1.814	0.0832	0.01141	140.7	-0.264	0.1028	0.513
26	-0.05745	1.503	0.0616	0.01091	164.2	-0.817	0.1183	0.488
27	-0.07944	1.477	0.0563	0.01177	172.4	-1.062	0.1314	0.482
28	-0.03175	1.509	0.0894	0.01075	170.4	-0.324	0.1159	0.436
29	-0.00649	1.675	0.0918	0.01100	154.6	-0.191	0.1069	0.410
30	-0.01570	1.477	0.3019	0.00396	170.3	2.569	0.0388	0.636
31	0.00090	2.014	0.3018	0.00531	139.2	2.571	0.0387	0.315
32	0.04053	6.083	0.3019	0.01438	108.6	2.573	0.0387	0.567

LIST OF FIGURES

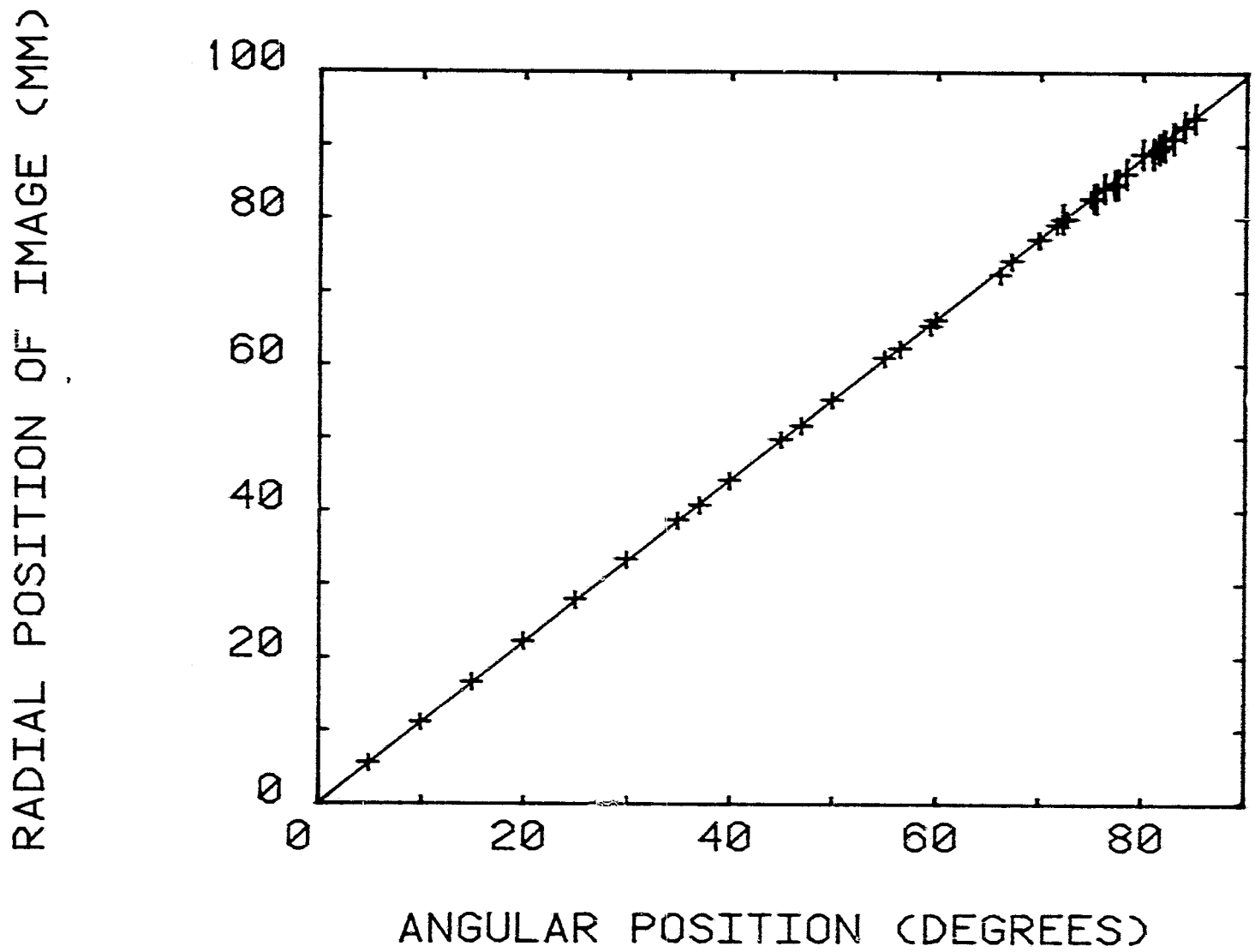

FIGURE 1. Whole-Sky Photographic System Calibration Plot. The distance of the image from the center of the photo is plotted versus the angular position. The error bars represent one standard deviation for each orientation for several points on each of two calibration photographs.

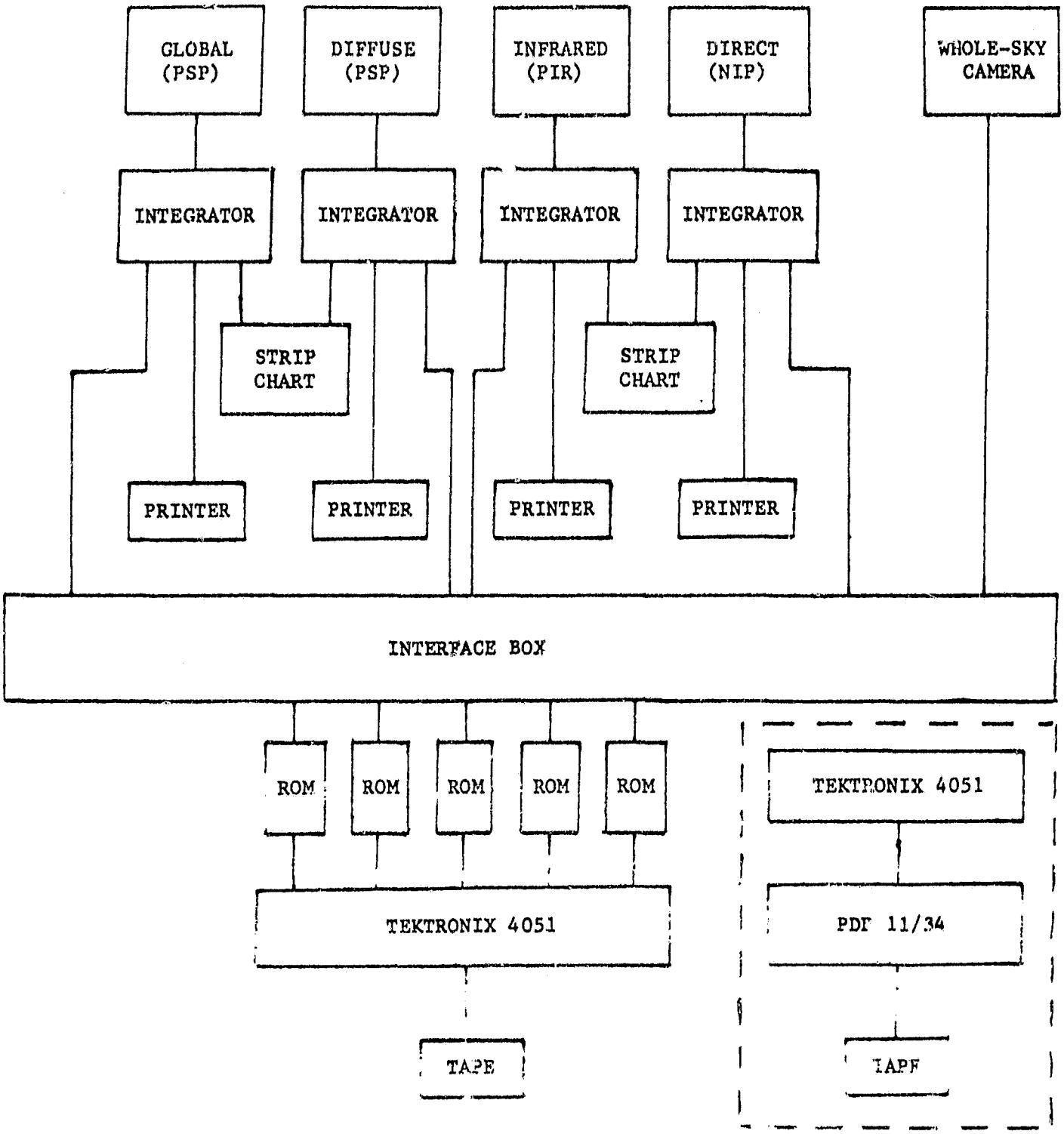

FIGURE 2. Automated Radiometric Data Acquisition System Flow Chart.

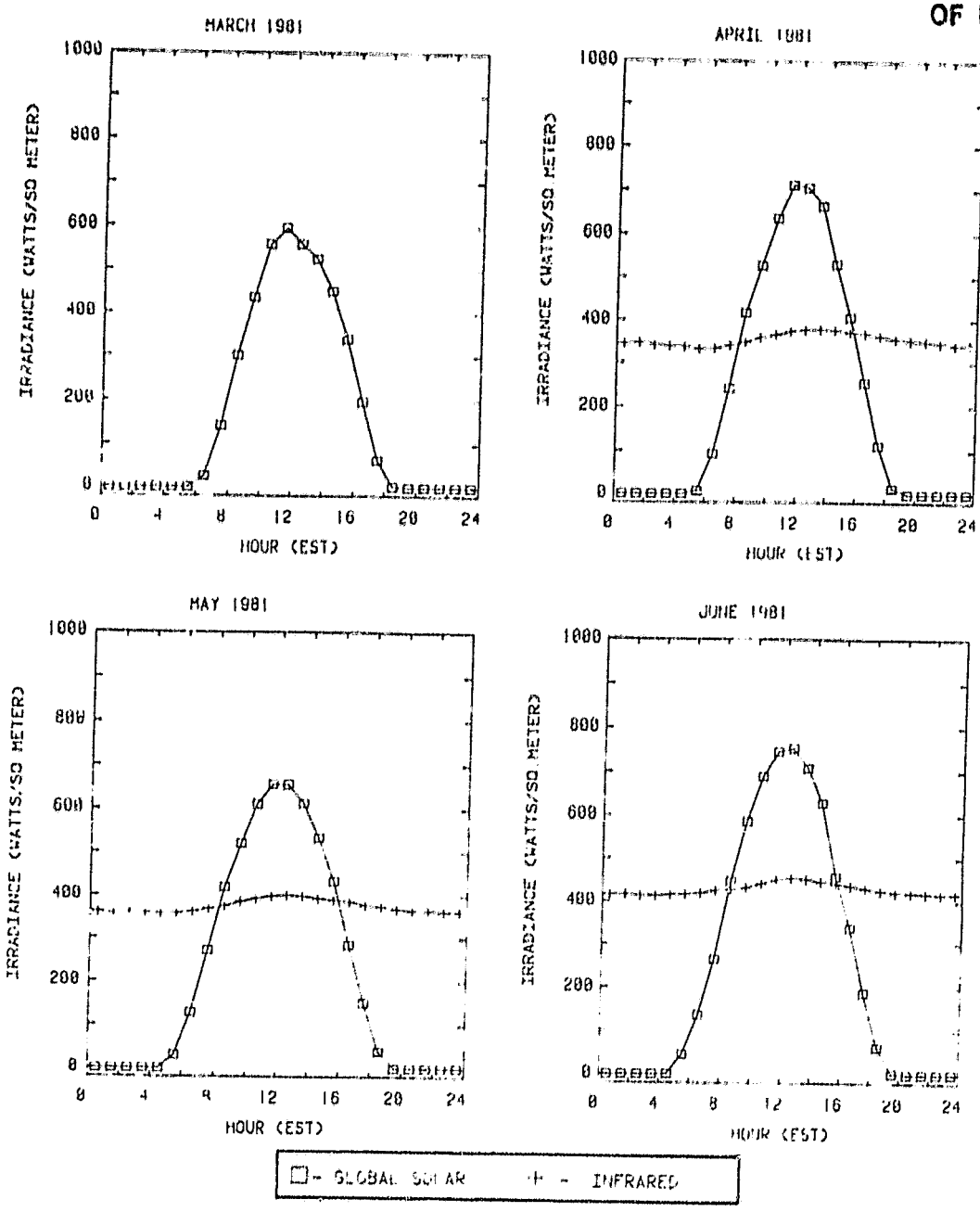

FIGURE 3. Average hourly ground irradiance and Atmospheric IR, Irradiance for Each Month from March thru June 1981.

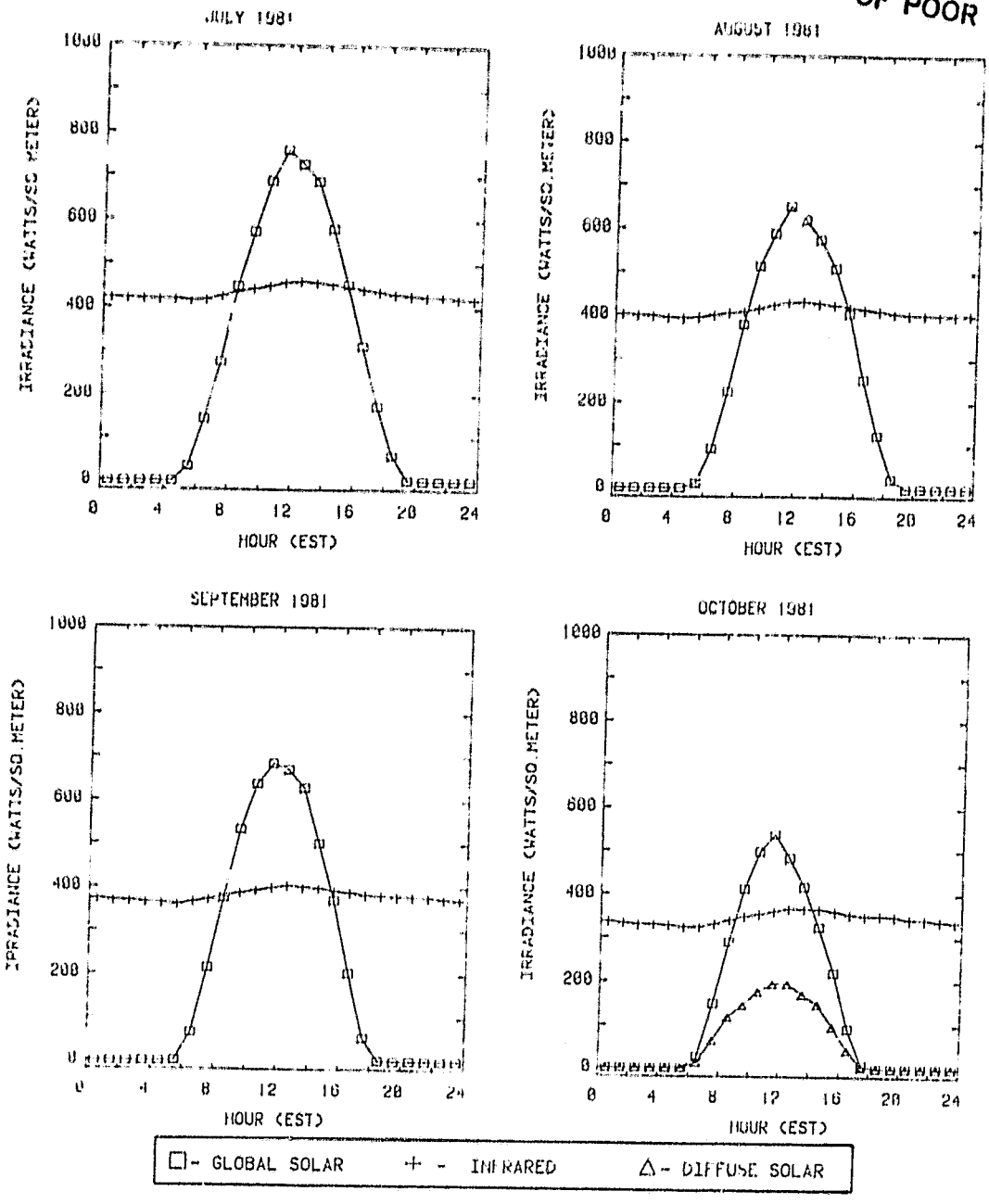

FIGURE 4. Average Hourly Global Irradiance and Atmospheric (IR) Emittance for Each Month from July thru October 1981. Diffuse solar irradiance is presented for October.

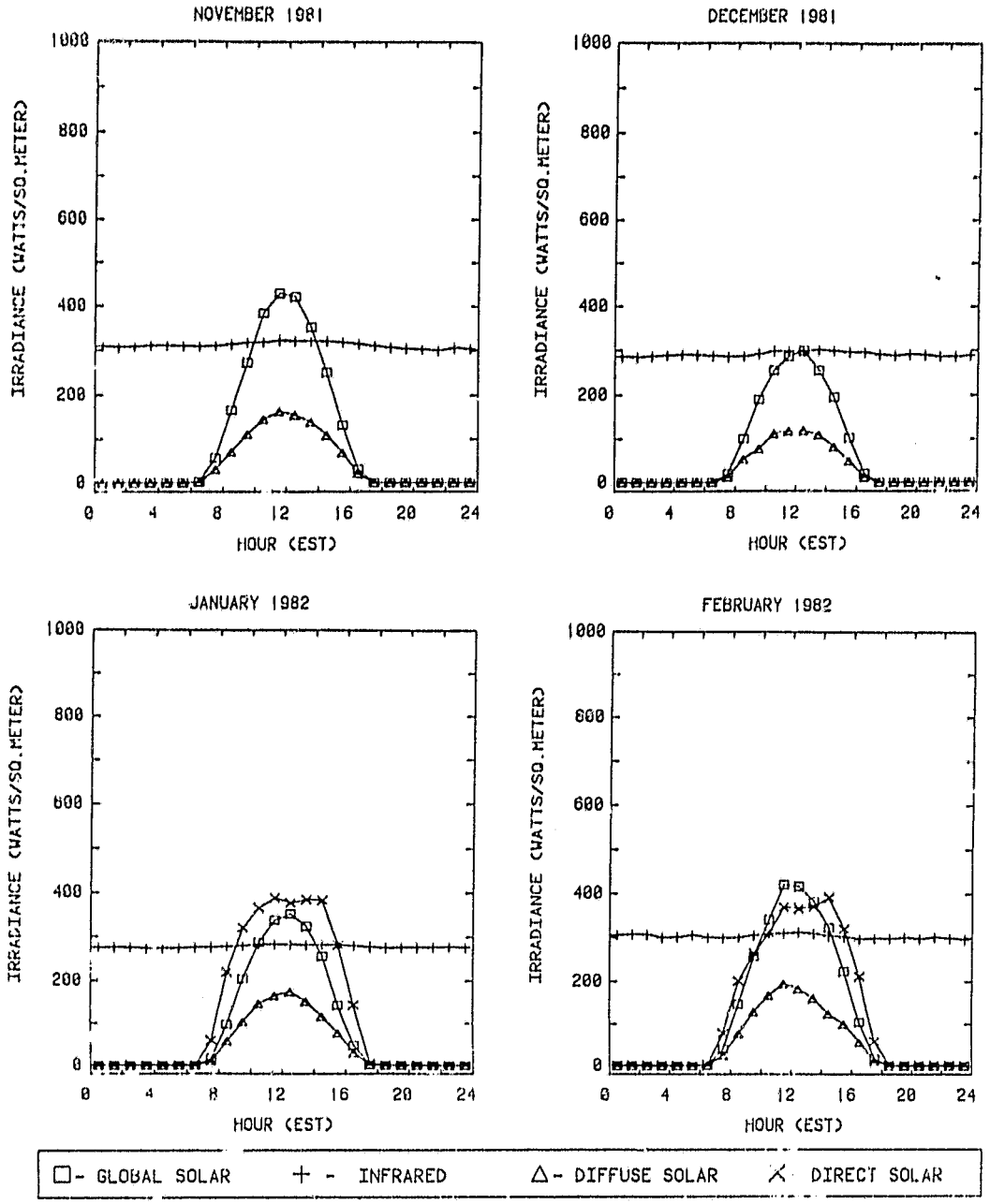

FIGURE 5. Average Hourly Global and Diffuse Solar Irradiances and Atmospheric (IR) Emittance for Each Month from November 1981 thru February 1982. Direct solar irradiance is plotted for January and February 1982.

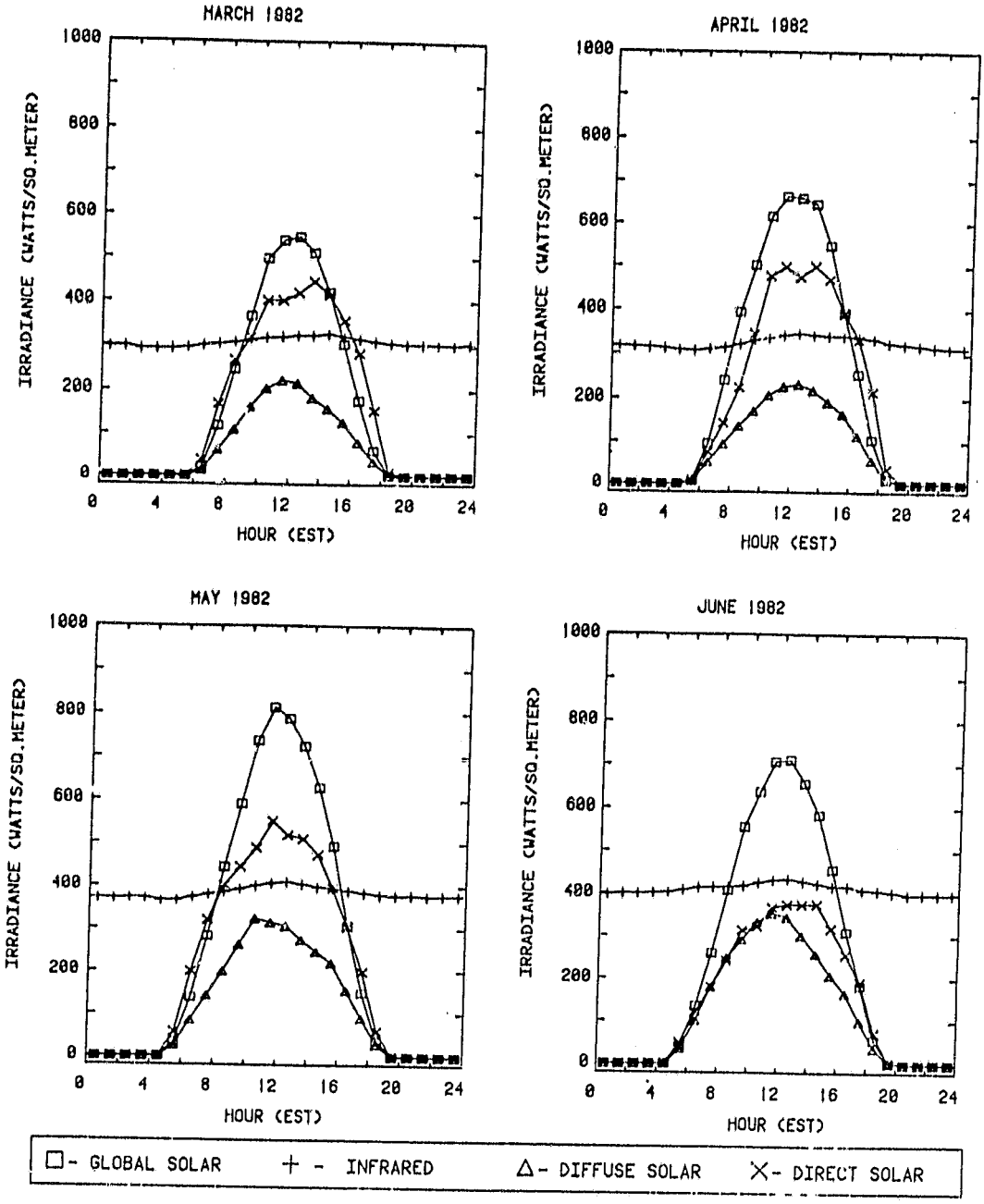

FIGURE 6. Average Hourly Global, Diffuse and Direct Solar Irradiances and Atmospheric (IR) Emittance for Each Month from March thru June 1982.

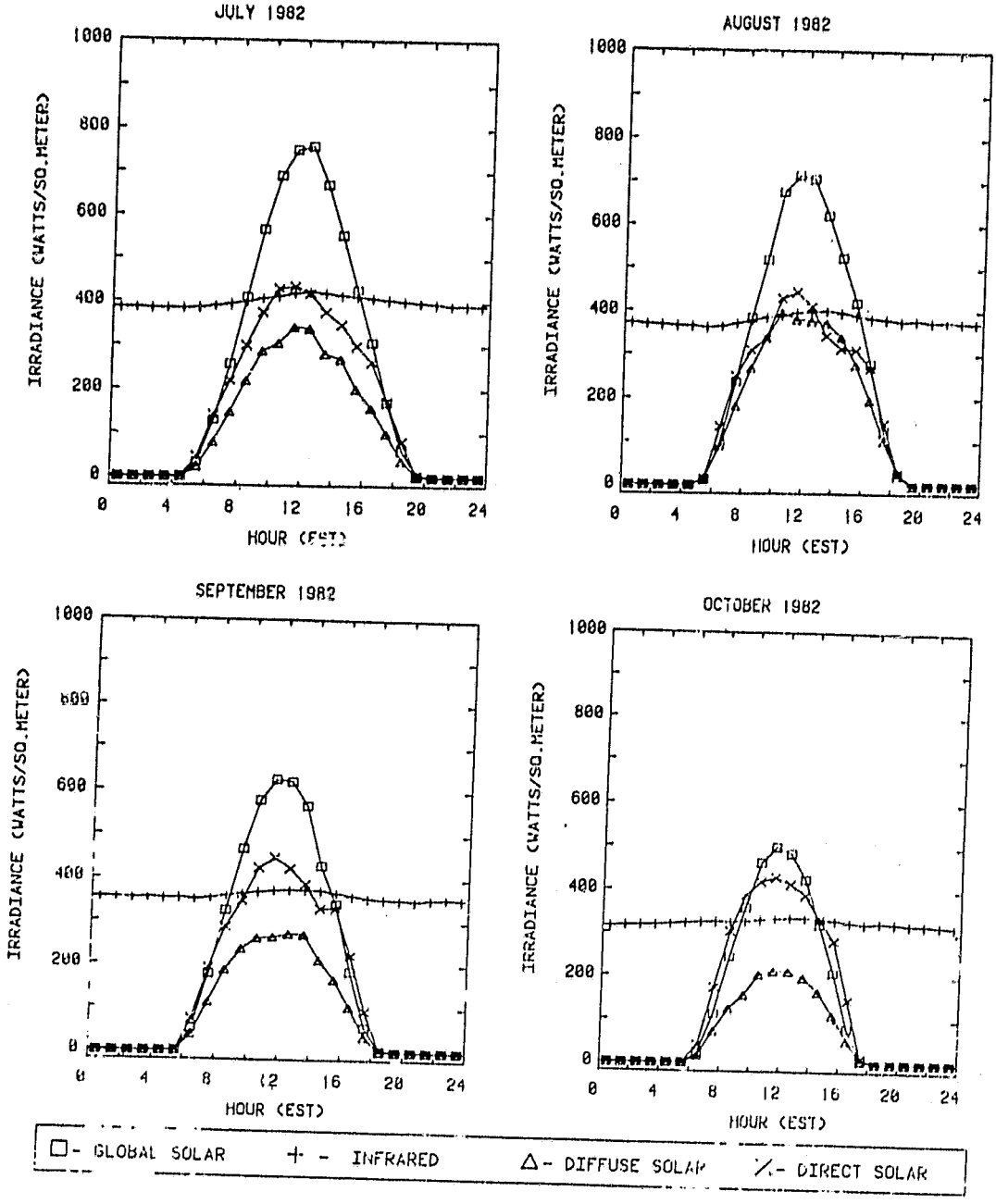

FIGURE 7. Average Hourly Global, Diffuse and Direct Solar Irradiances and Atmospheric (IR) Emittance for Each Month from July thru October 1982.

ORIGINAL PAGE IS
OF POOR QUALITY

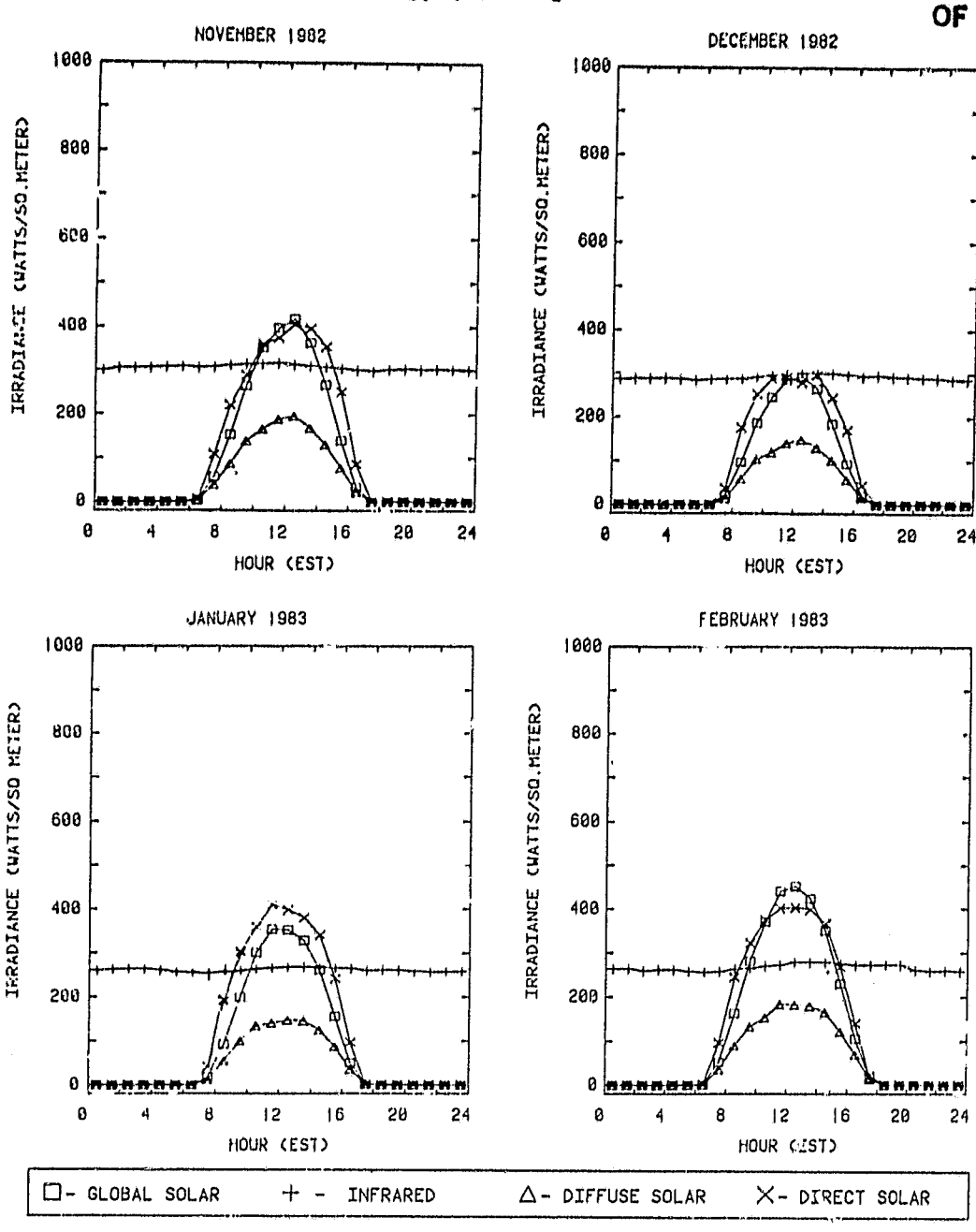

FIGURE 8. Average Hourly Global, Diffuse and Direct Solar Irradiances and Atmospheric (IR) Emittance for Each Month from November 1982 thru February 1983.

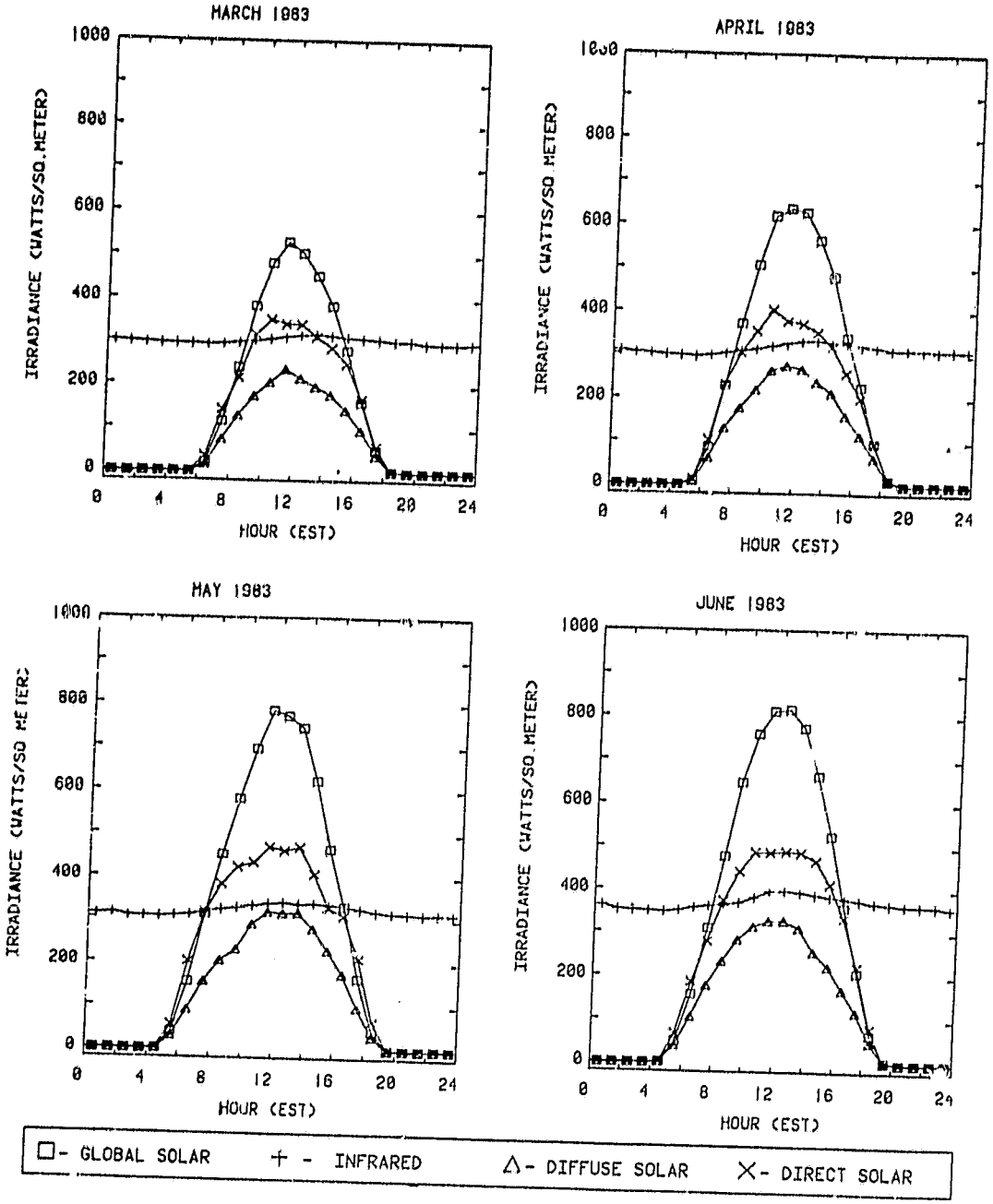

FIGURE 9. Average Hourly Global, Diffuse and Direct Solar Irradiances and Atmospheric (IR) Emittance for Each Month from March thru June 1983.

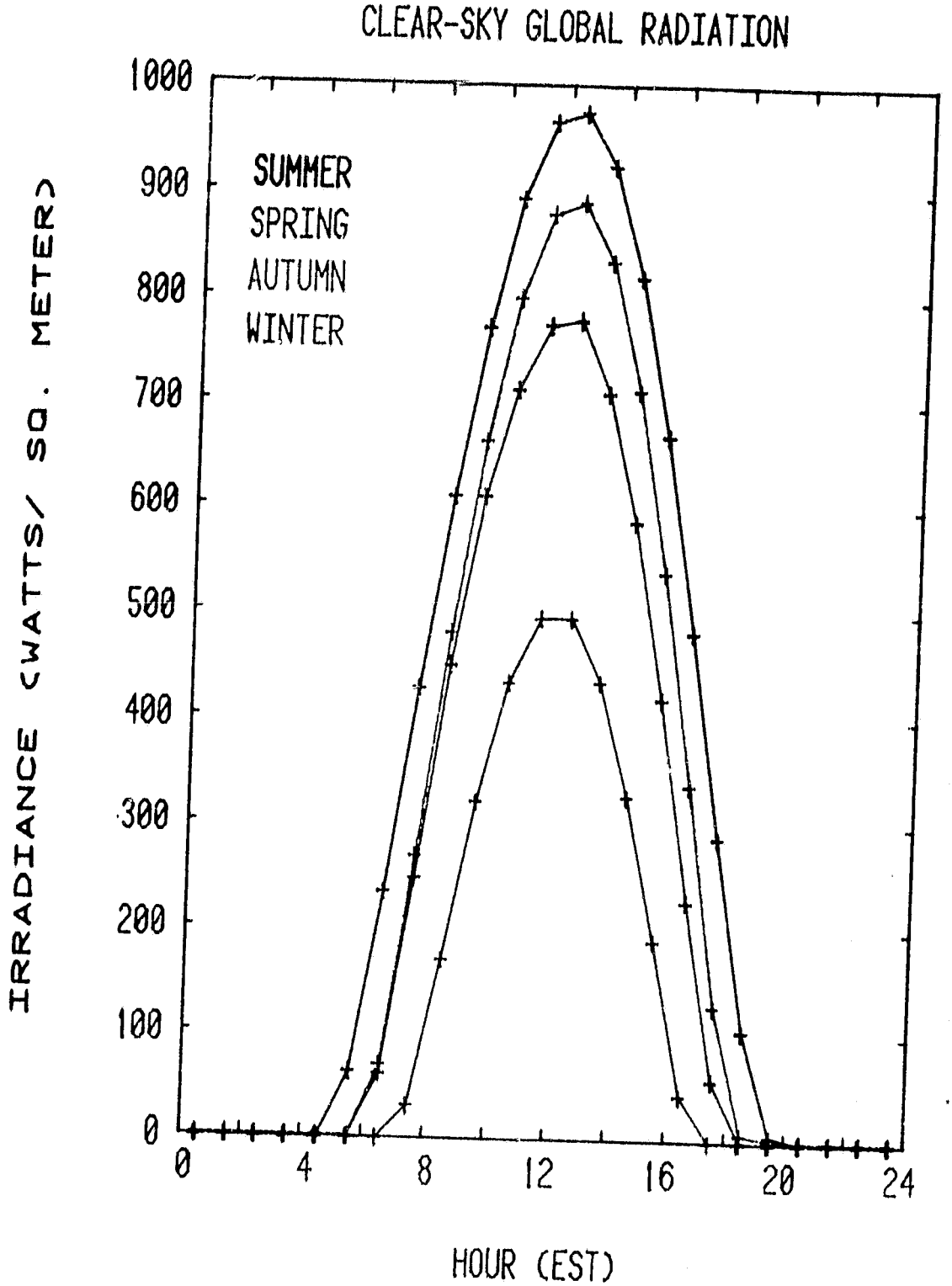

FIGURE 10. Seasonal Variability of Clear-Sky Global Irradiance for Selected Days.

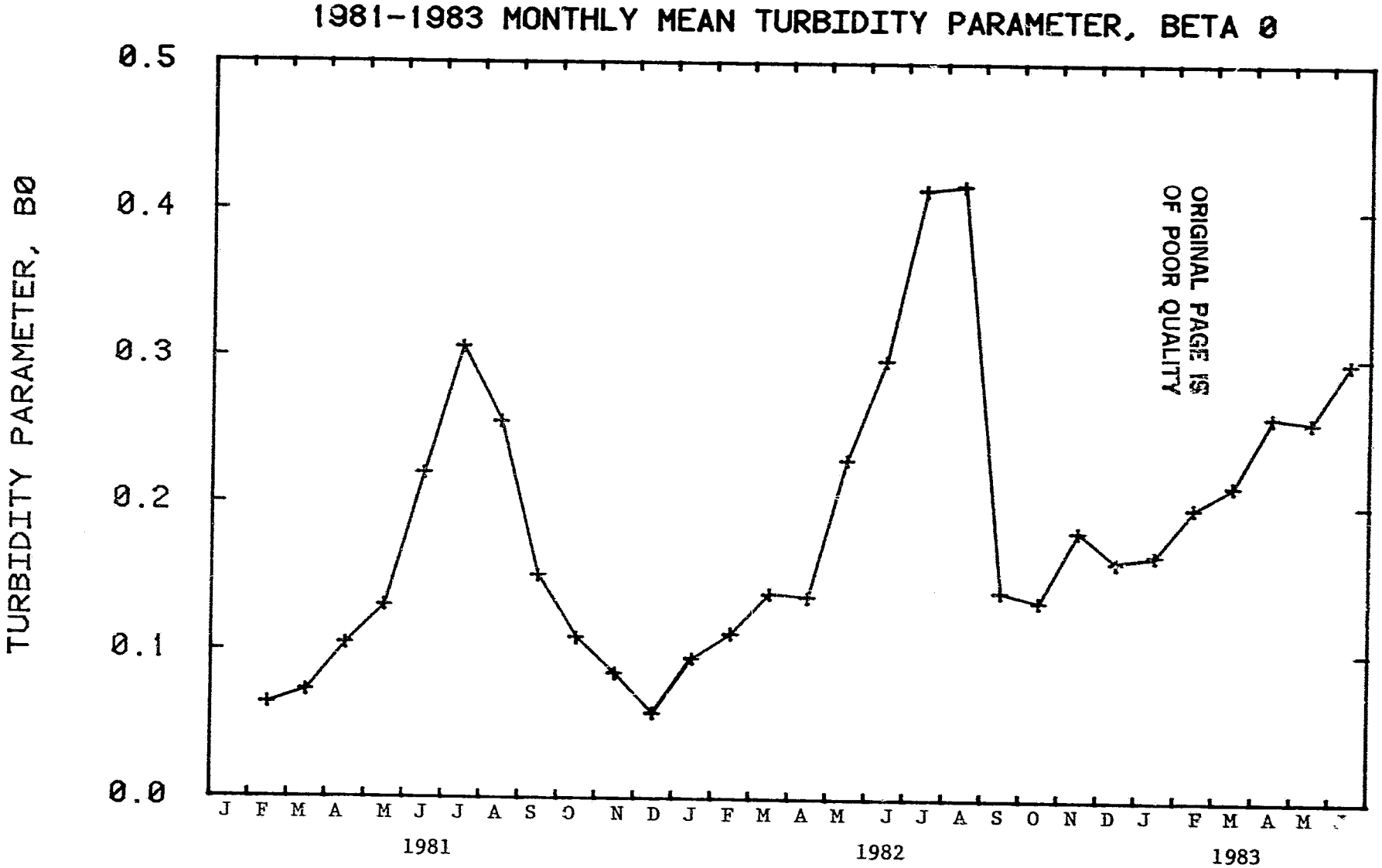

FIGURE 11. Monthly Average Ångström Turbidity Coefficient β_o for the period March 1981 thru June 1983.

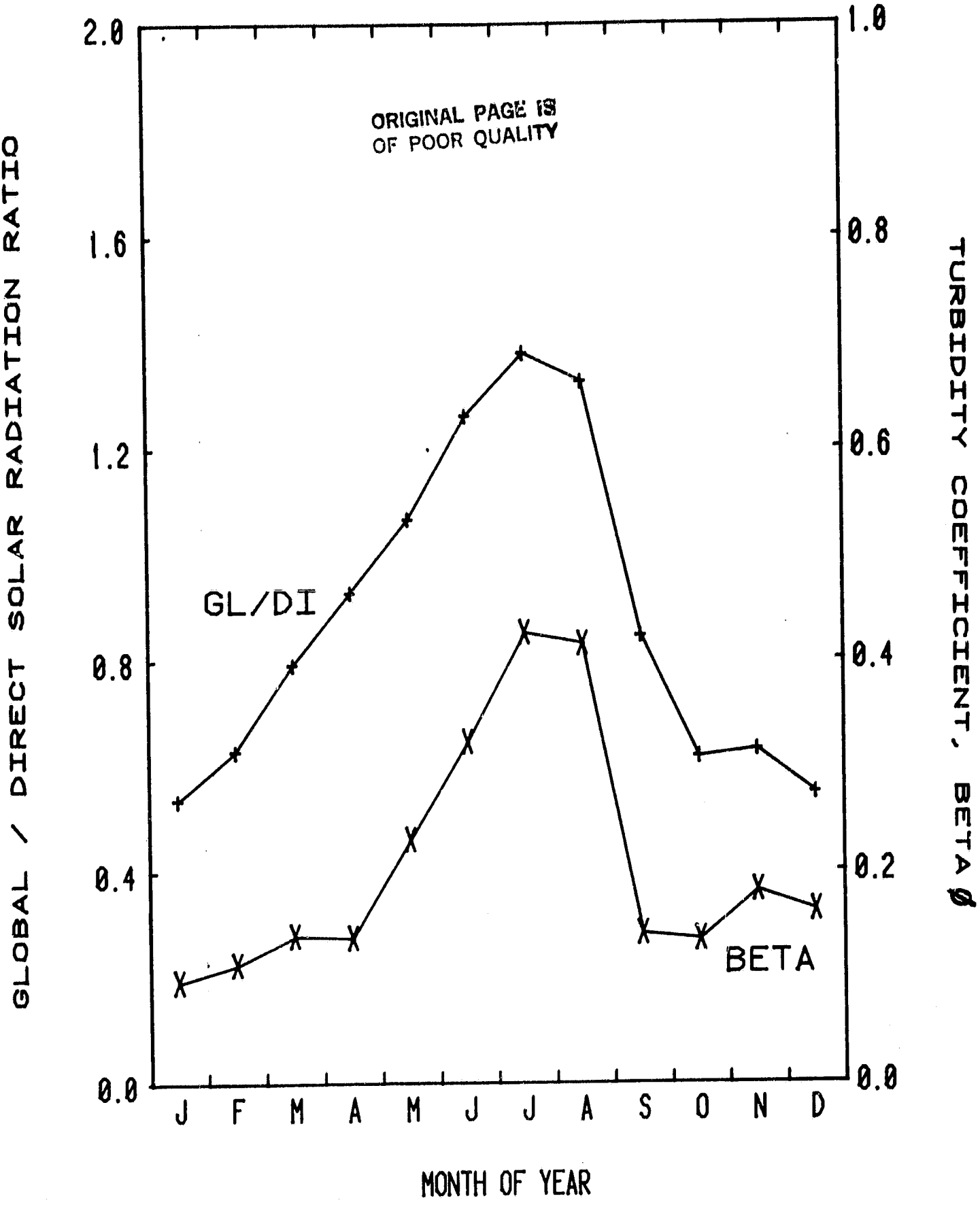

FIGURE 12. Global to Direct Solar Irradiance Ratio and Turbidity Coefficient β for the 1982 Calendar Year. Irradiance values for the hour containing each turbidity measurement were used for each ratio.

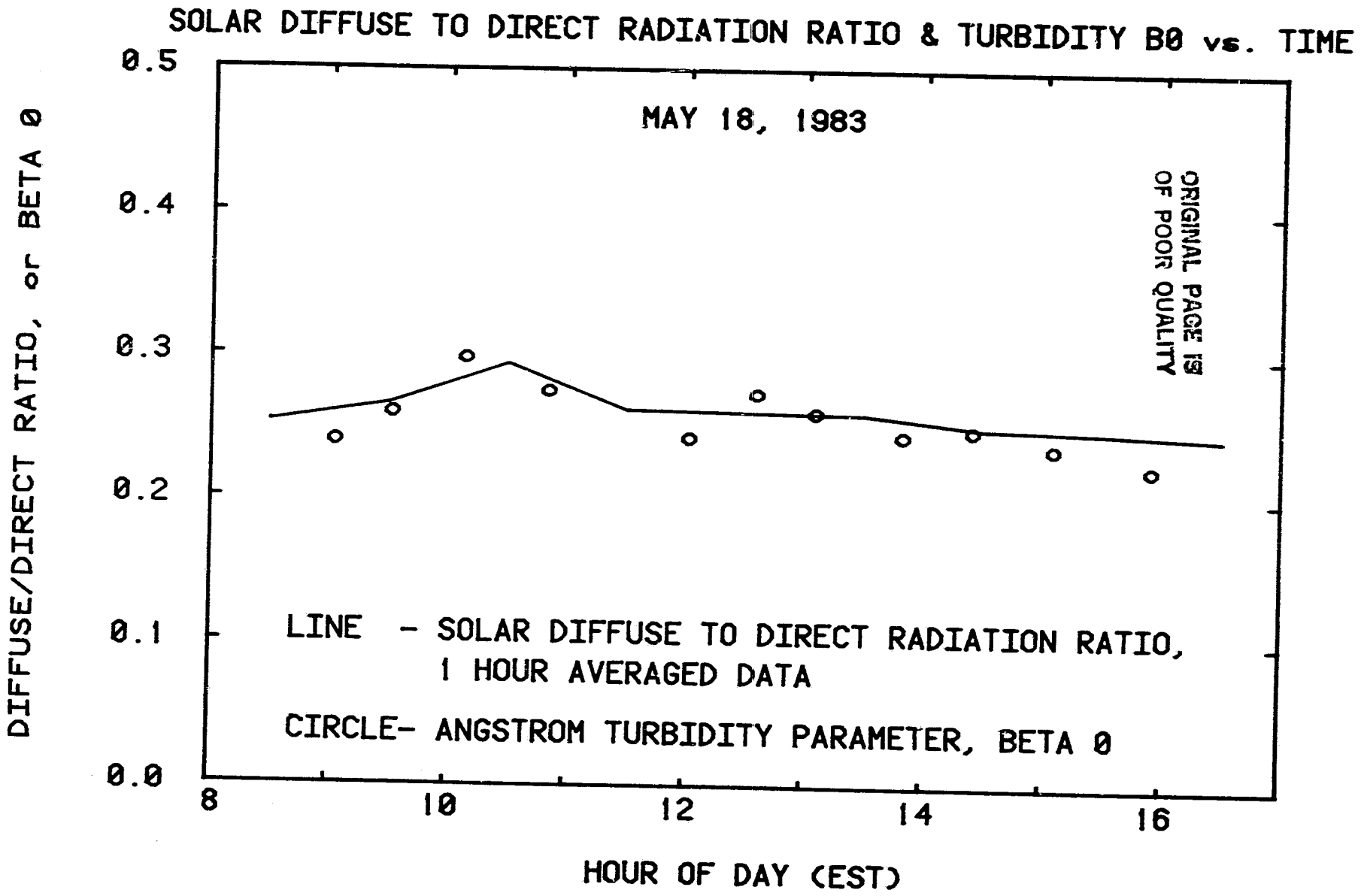

FIGURE 13. Diffuse to Direct Solar Irradiance Ratio and Turbidity Coefficient β_o for May 18, 1983. Irradiance values for the hour containing each turbidity measurement were used for each ratio.

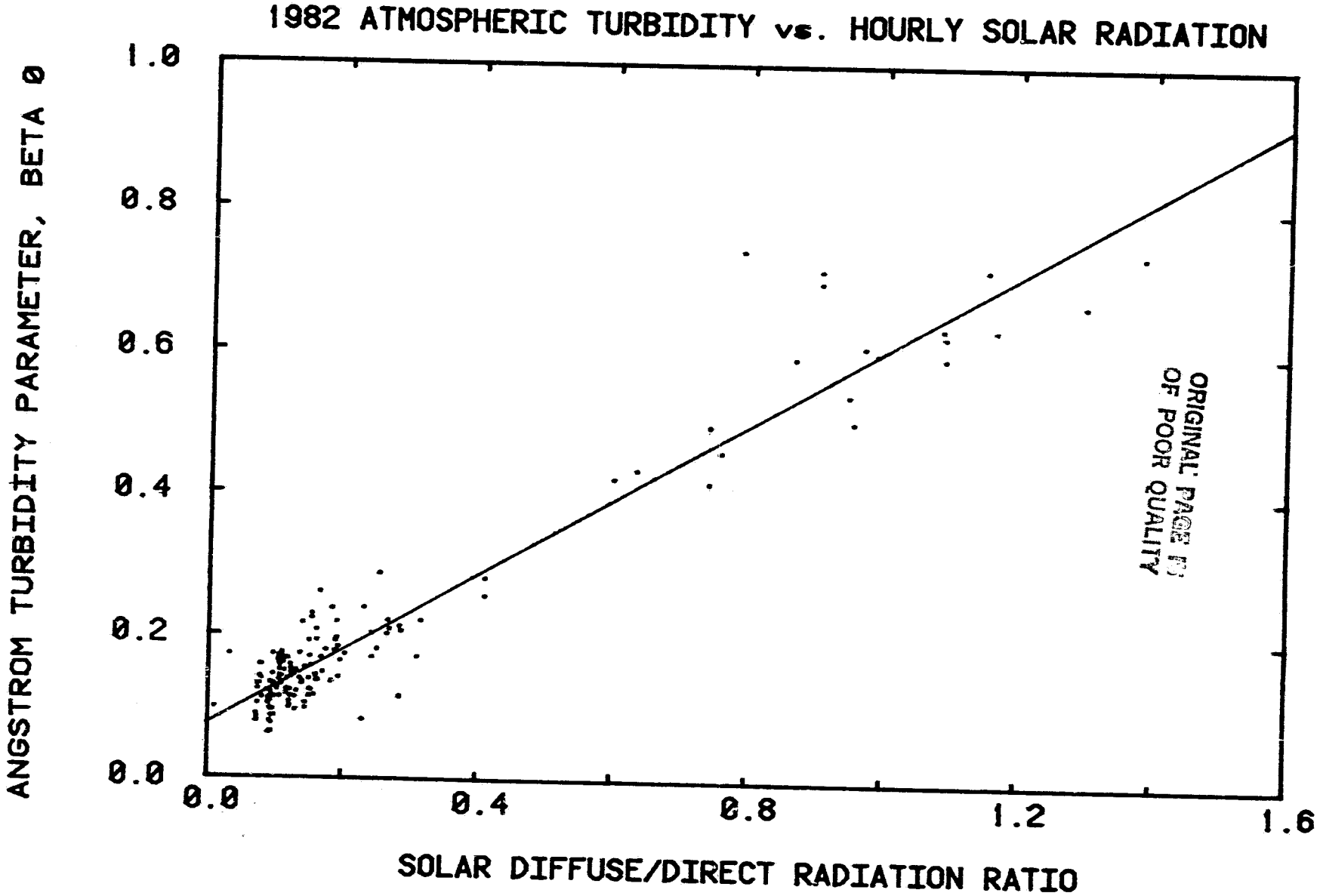

FIGURE 14. Turbidity Coefficient β versus Diffuse to Direct Solar Irradiance Ratio. Irradiance values for the hour containing each turbidity measurement are compared to β_o for all measurements during the 1982 calendar year.

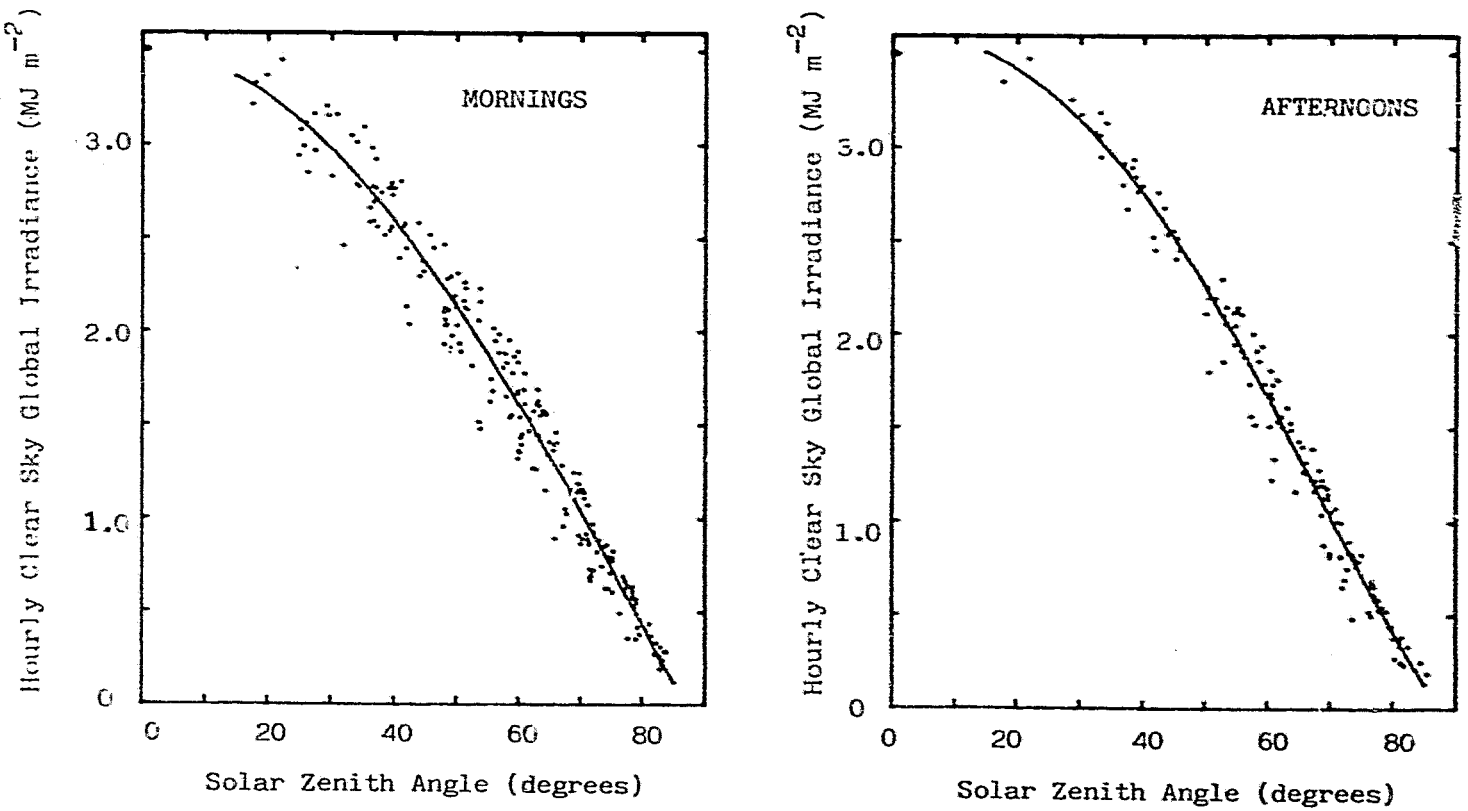

ORIGINAL PAGE IS
OF POOR QUALITY

FIGURE 15. Clear Sky Global Insolation versus Solar Zenith Angle. The data for mornings are plotted at the left and for afternoons at the right for the one year period March 1981 thru February 1982. The curve represents the result of the least squares fit to equation 1 for each data set.

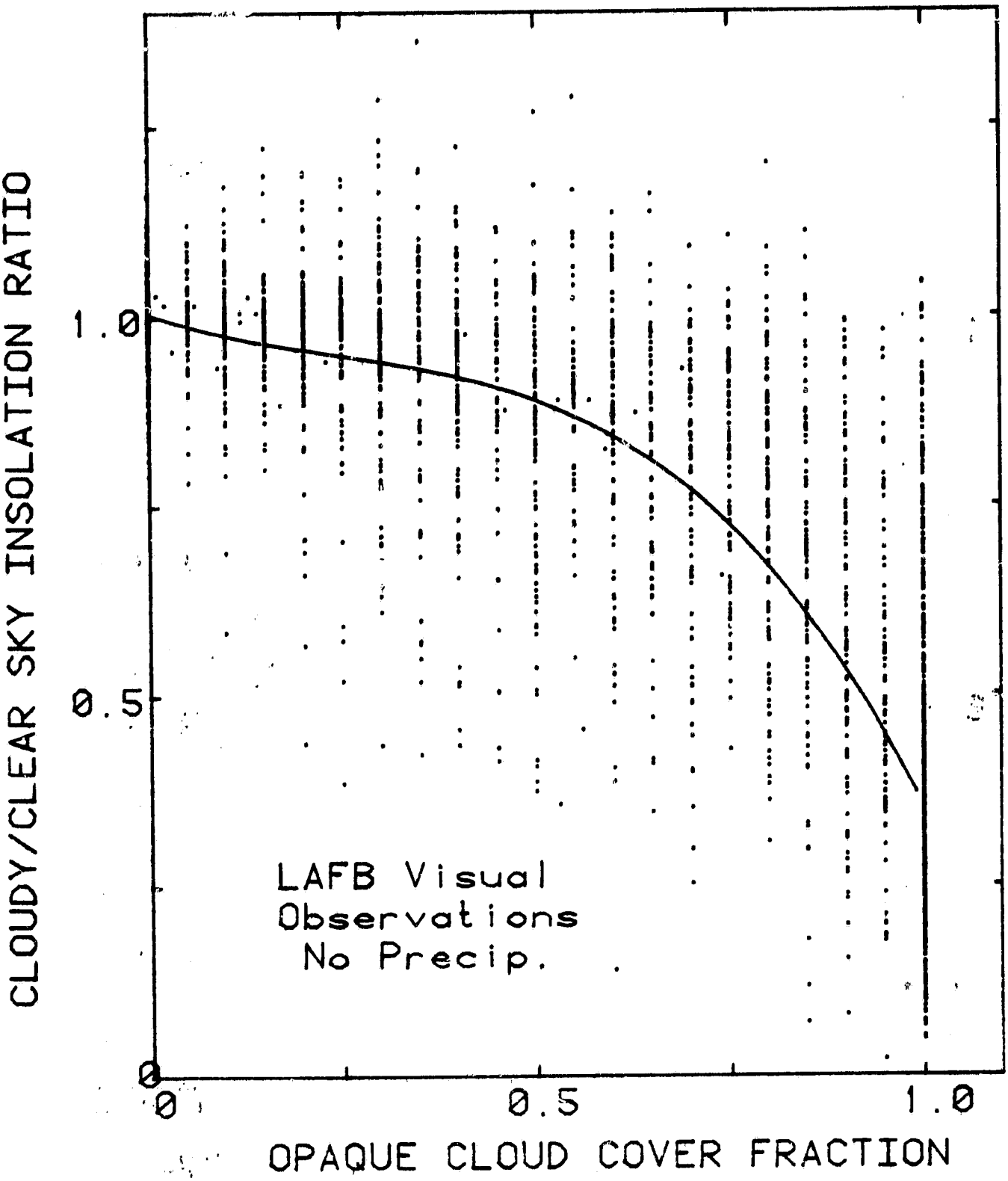

FIGURE 16. Cloudy to Clear Sky Global Insolation Ratio Versus Cloud Cover Fraction-Visual Estimates. Each hourly insolation value was normalized by the expected clear sky value. Cloud cover fractions are averages of the hourly visual observations made at Langley Air Force Base. The curve is the result of a least squares fit to equation 2.

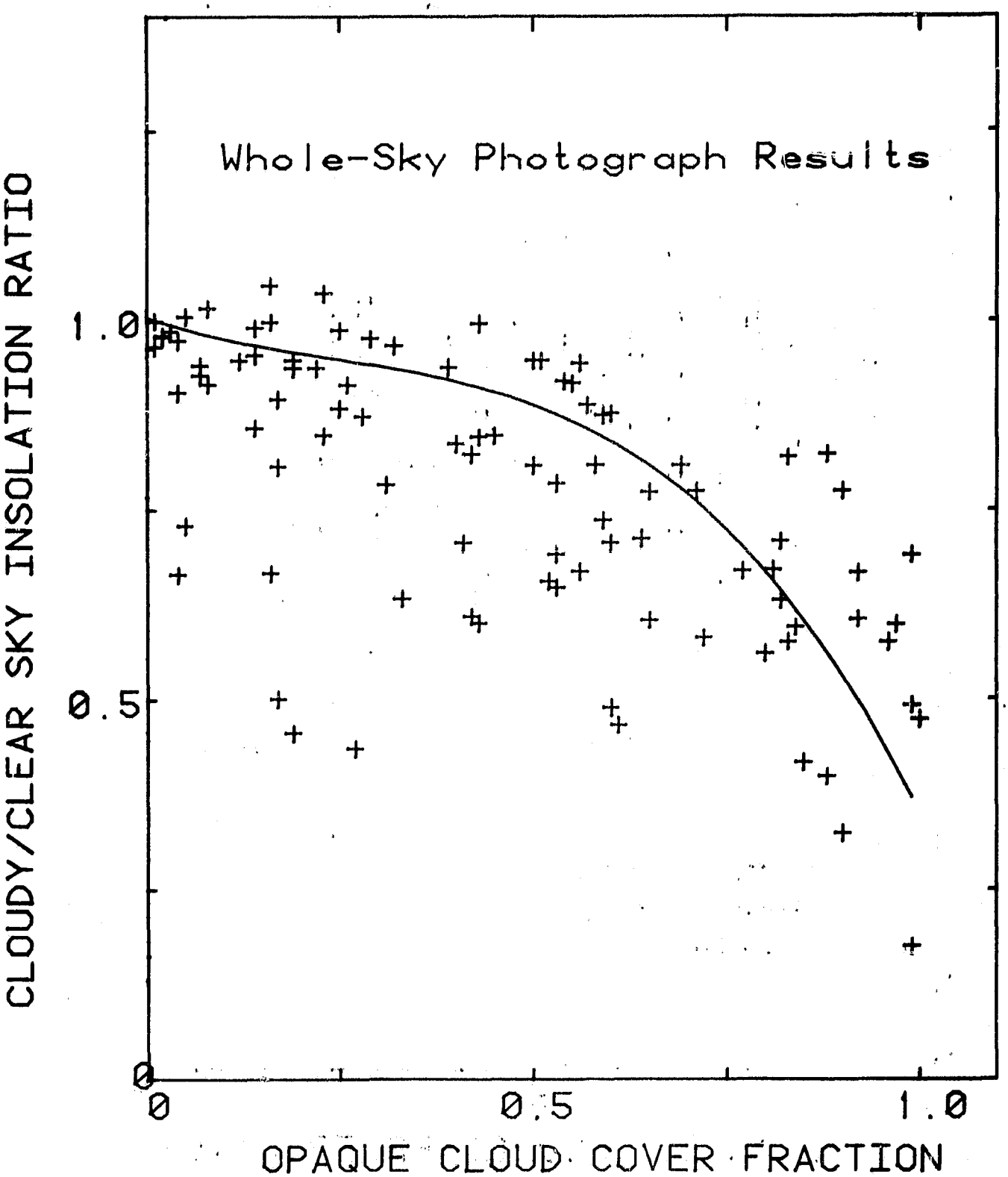

FIGURE 17. Cloudy to Clear Sky Global Insolation Ratio Versus Cloud Cover Fraction-Whole Sky Photographs. Each hourly insolation value was normalized by the expected clear sky value. The cloud cover fractions were obtained by analysis of black and white prints and of color slides of the local sky. The curve represents the result of the least squares fit to equation 2 using the LAFB data set.

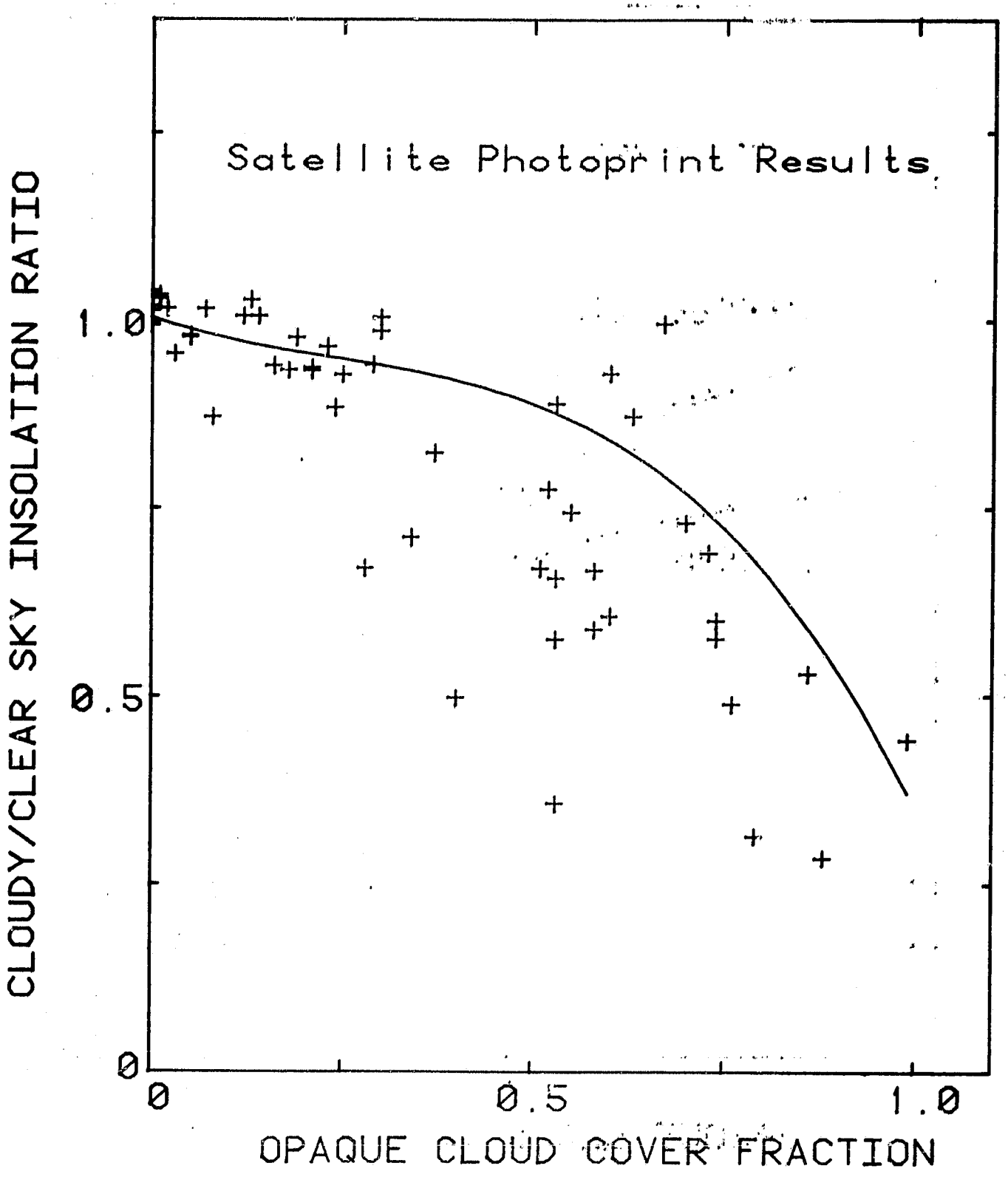

FIGURE 18. Cloudy to Clear Sky Global Insolation Ratio Versus Cloud Cover Fraction-Satellite Photoprints. Each hourly insolation value was normalized by the expected clear sky value. The cloud cover fractions were obtained by the analysis of GOES-East photoprints. The curve represents the result of the least squares fit to equation 2 using the LAFB data set.

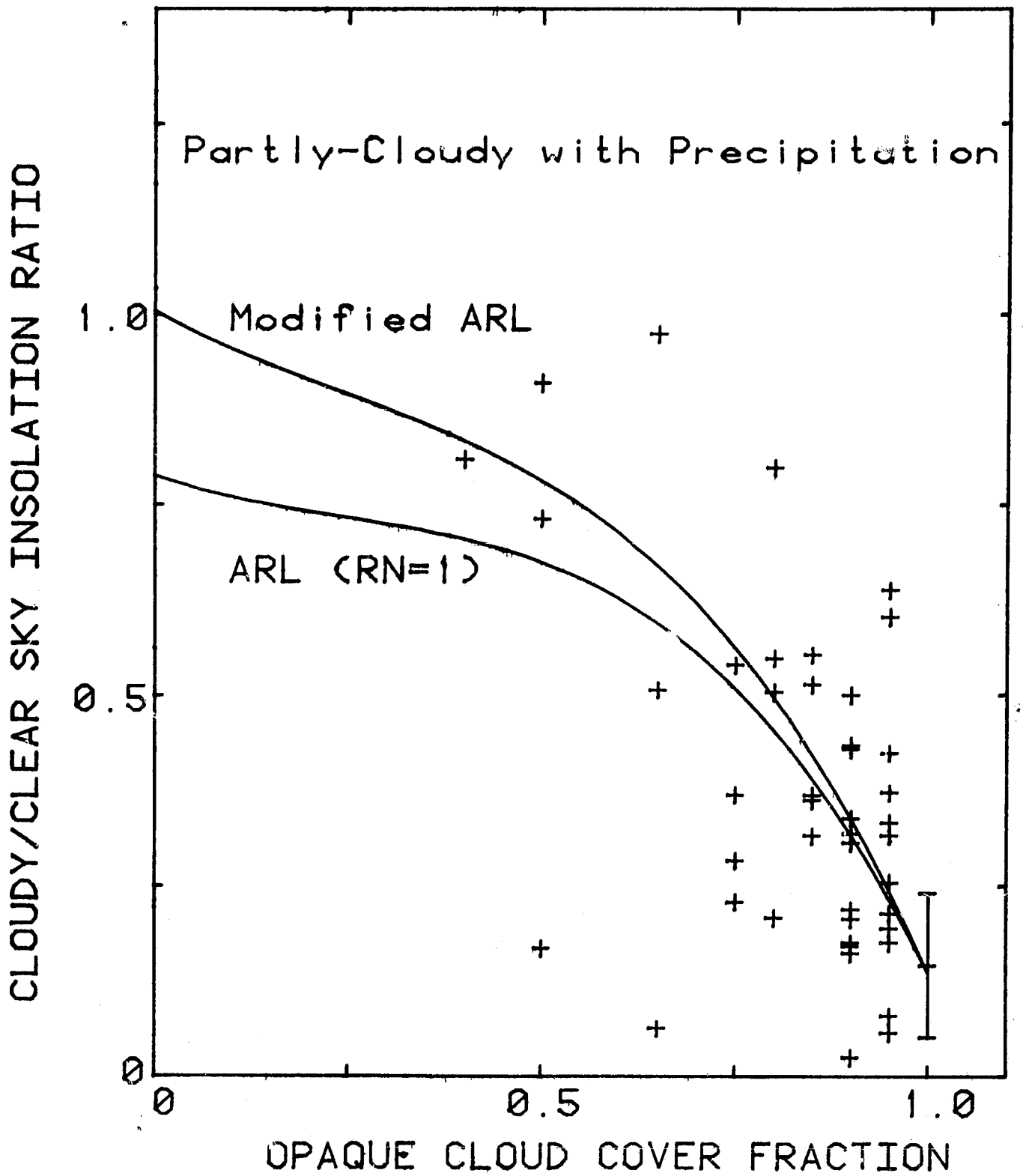

FIGURE 19. Cloudy to Clear Sky Global Insolation Ratio Versus Cloud Cover Fraction-with Precipitation Present. Each hourly insolation value was normalized by the expected clear sky value. The cloud cover fractions are averages of visual observations at nearby LAFB. The lower curve is the same curve as used in FIGURES 16-18 with the rain term RN set equal to 1. The upper curve has the same coefficients but modifies the rain term by a factor of OPQ.

FIGURE 20. Hampton Institute Study Region and Local Meteorological Data Sources

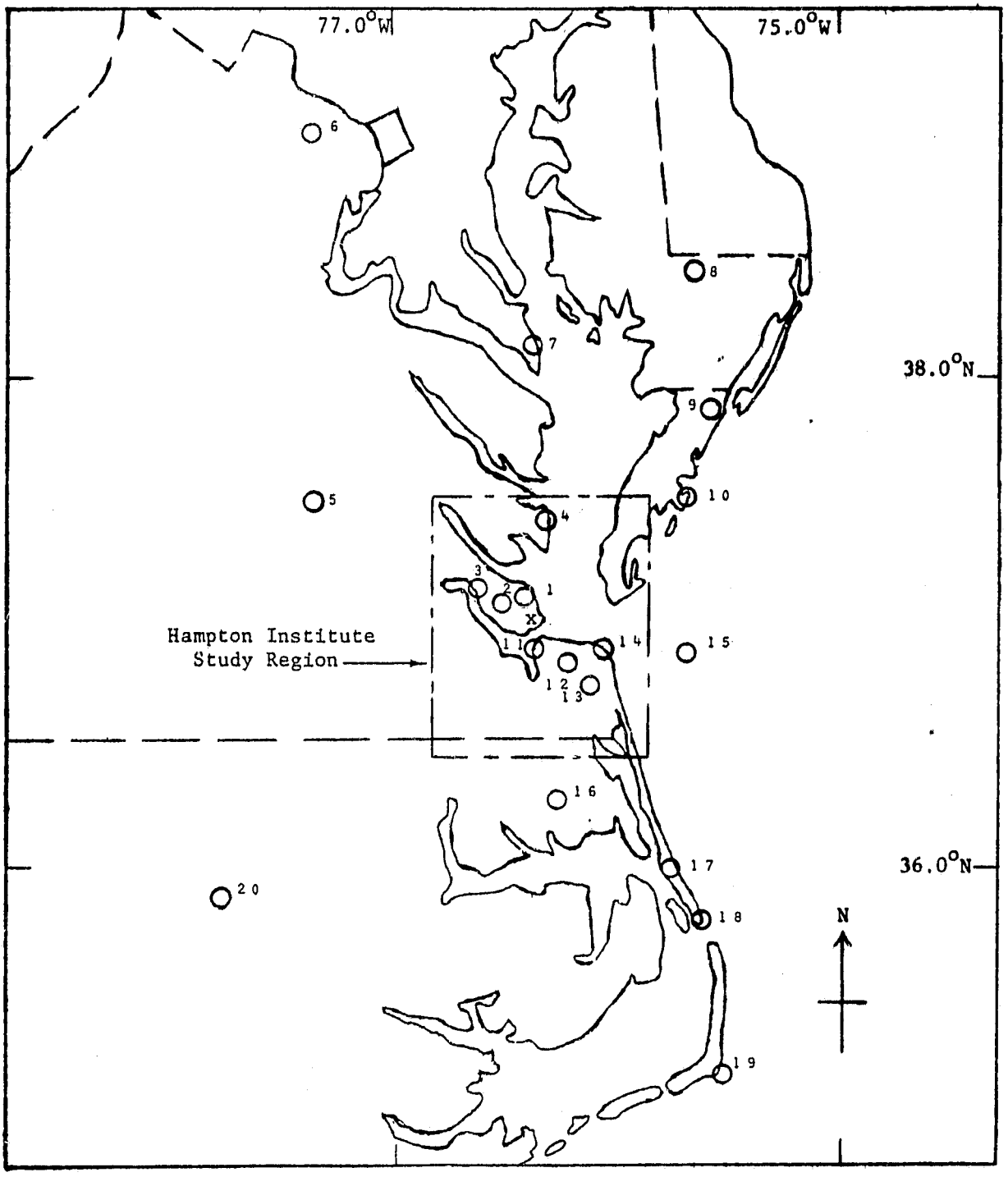

Legend

X- Hampton Institute
1- Langley A.F.B.
2- Newport News, VA
3- Fort Eustis, VA
4- Milford Haven, VA
5- Richmond, VA
6- Sterling, VA
7- Patuxent River,MD
8- Salisbury, MD
9- Wallops Island, VA
10- Paramore Beach, VA
11- Navel Air Norfolk,VA
12- Norfolk, VA
13- Oceana Navel Air, VA
14- Cape Henry, VA
15- Chesapeake Lighthouse
16- Elizabeth City, NC
17- Dare County, NC
18- Oregon Inlet, NC
19- Cape Hatteras, NC
20- Rocky Mount, NC

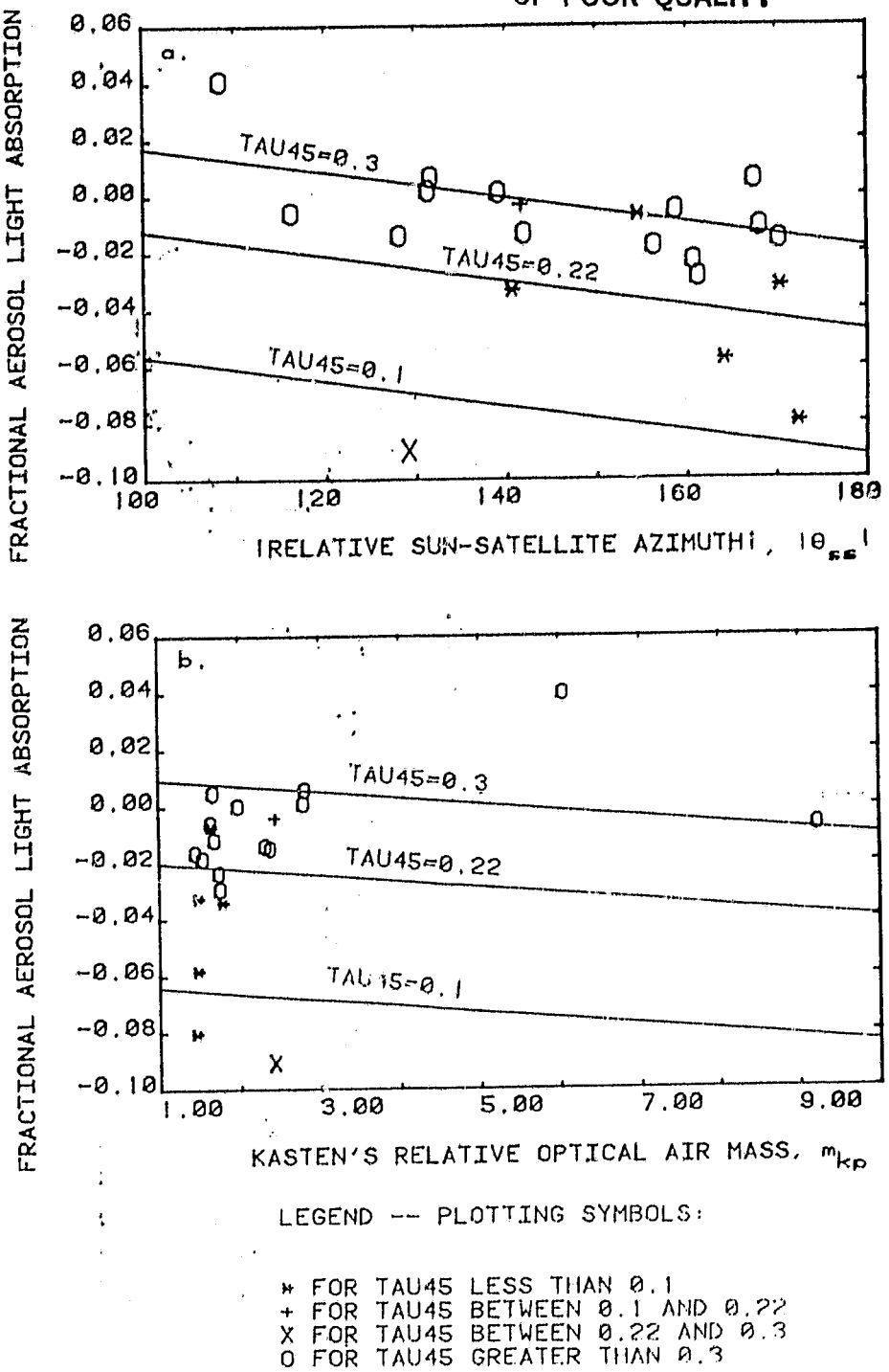

FIGURE 21. Fractional Aerosol Light Absorption as a function of: (upper plot) Relative Sun-Satellite Azimuth, θ_{ss}; and, (lower plot) Kasten's Relative Optical Air Mass, m_{kp}.

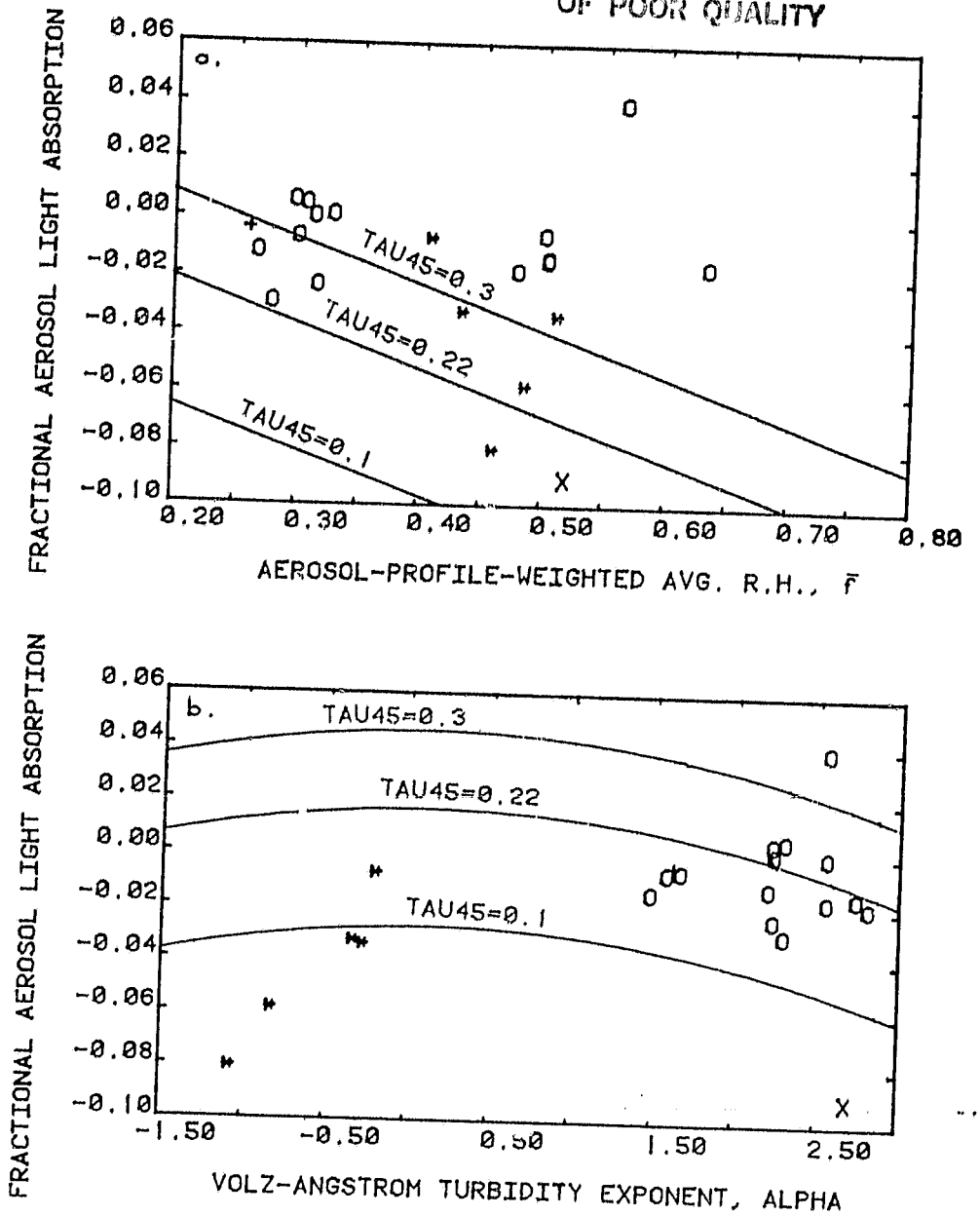

FIGURE 22. Fractional Aerosol Light Absorption as a Function of: (upper plot) Aerosol-Profile Weighted Mean Relative Humidity, $\bar{f}$; and, (lower plot) Volz-Ångström Turbidity Exponent, α.

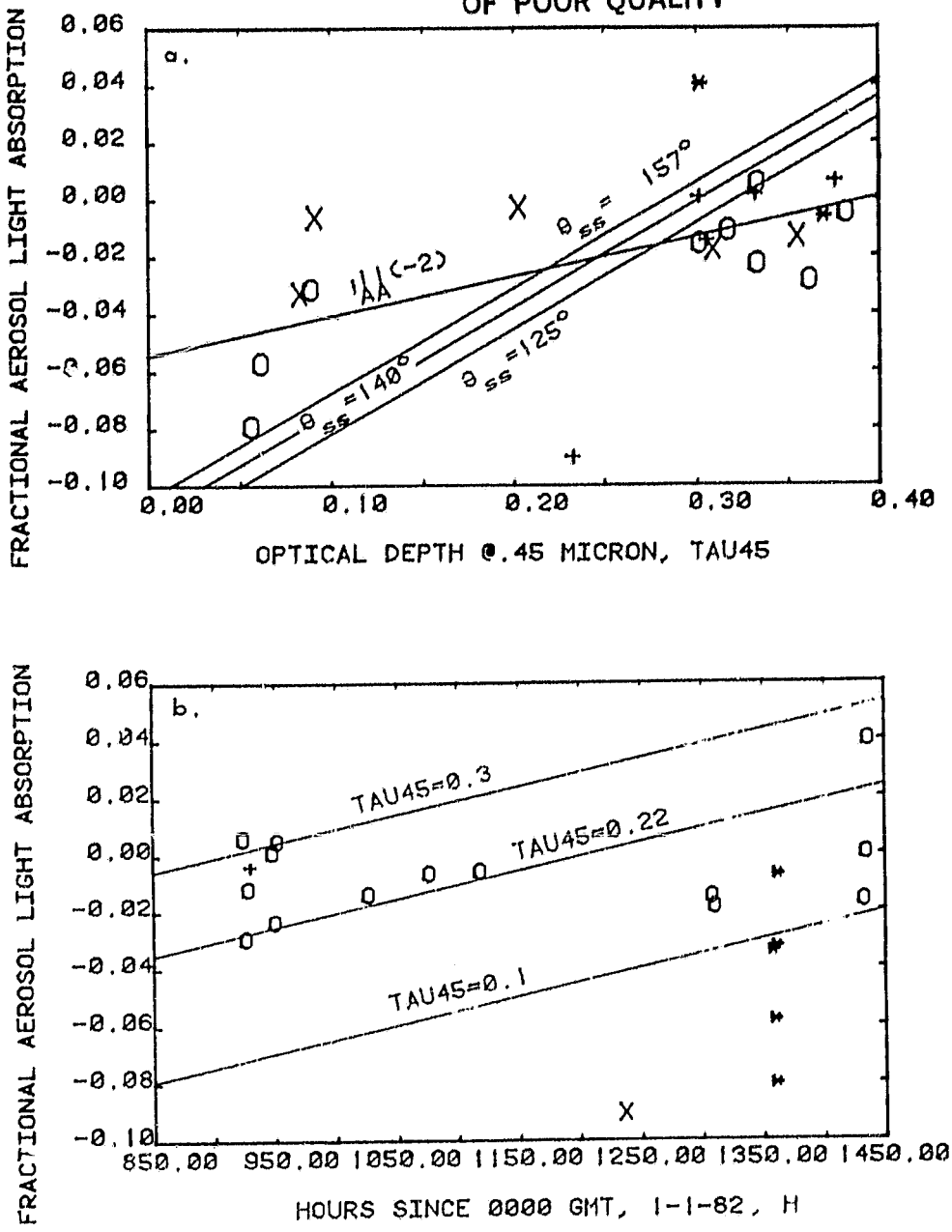

LEGEND -- PLOTTING SYMBOLS:

FOR a.: * FOR θ_{SS} LESS THAN 125°
+ FOR θ_{SS} BETWEEN 125° AND 140°
X FOR θ_{SS} BETWEEN 140°AND 157°
O FOR θ_{SS} GREATER THAN 157°

FOR b.: * FOR TAU45 LESS THAN 0.1
+ FOR TAU45 BETWEEN 0.1 AND 0.22
X FOR TAU45 BETWEEN 0.22 AND 0.3
O FOR TAU45 GREATER THAN 0.3

FIGURE 23. Fractional Aerosol Light Absorption as a Function of: (upper plot) Optical Depth at a Wavelength of 0.45 μm; and, (lower plot) Hours since 0000 GMT, January 8, 1982.

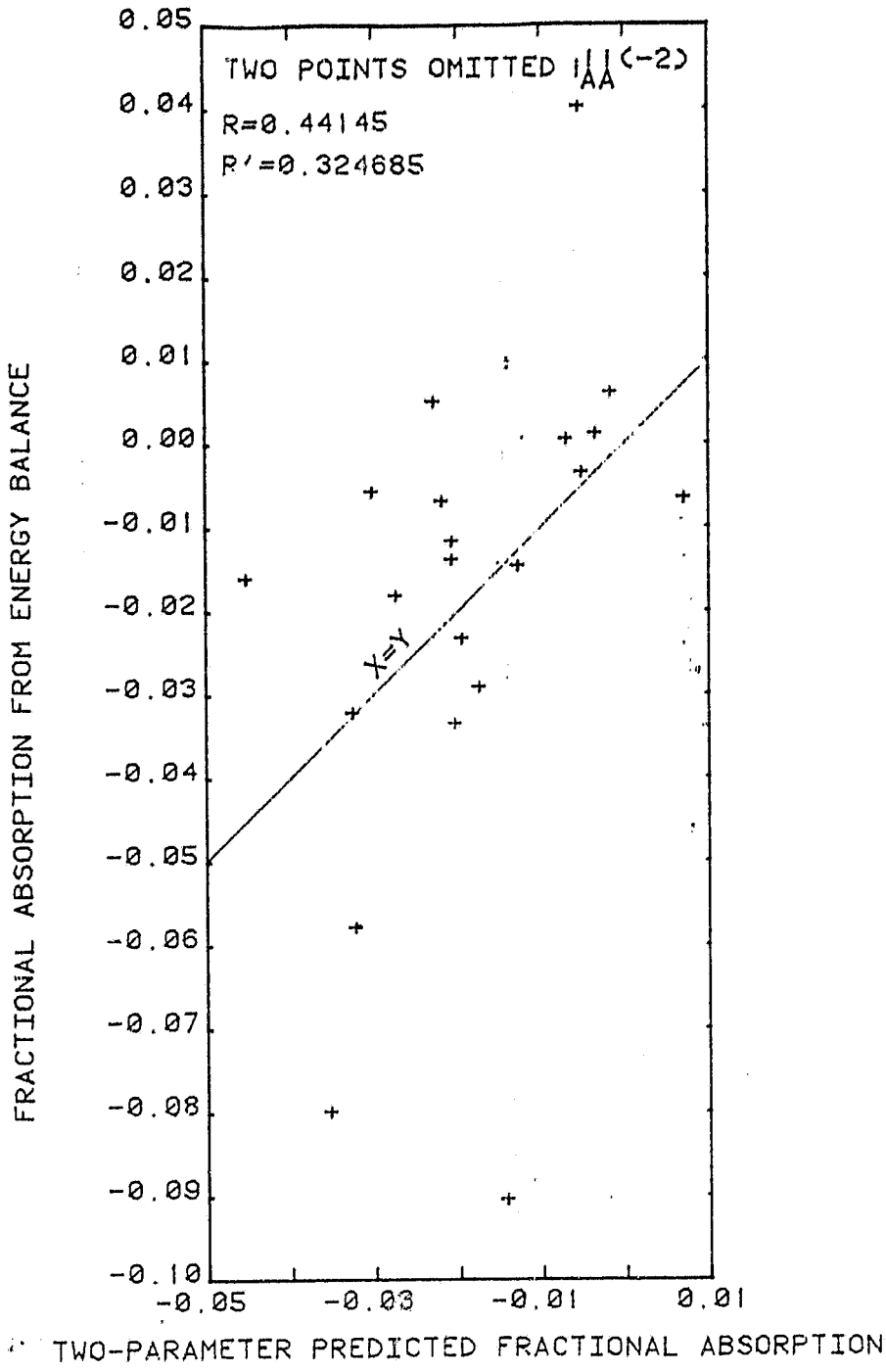

FIGURE 24. Scatter Diagram of Fractional Light Absorption by Aerosols Estimated from Energy Balance Versus Predicted Absorption for Case 1.i. The fractional light absorption by aerosols was predicted by a least - squares-fit formula derived from the data set having two cases and all turbidity related parameters excluded.

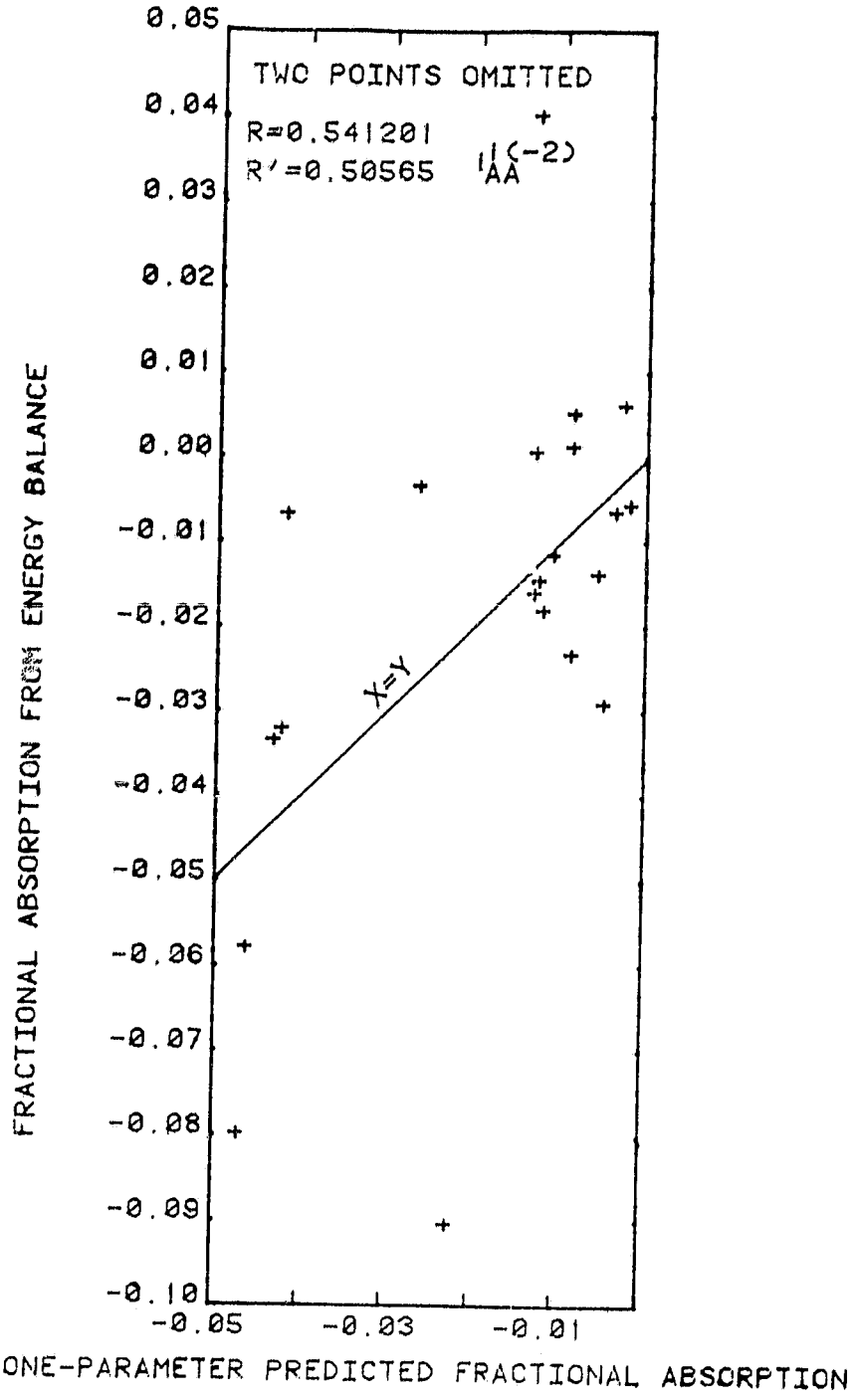

FIGURE 25. Scatter Diagram of Fractional Light Absorption by Aerosols Estimated from Energy Balance Versus Predicted Absorption for Case 1.ii(a). The fractional light absorption by aerosols was predicted by a least-squares-fit formula derived from the data set having two cases excluded and with $p \geq 68\%$.

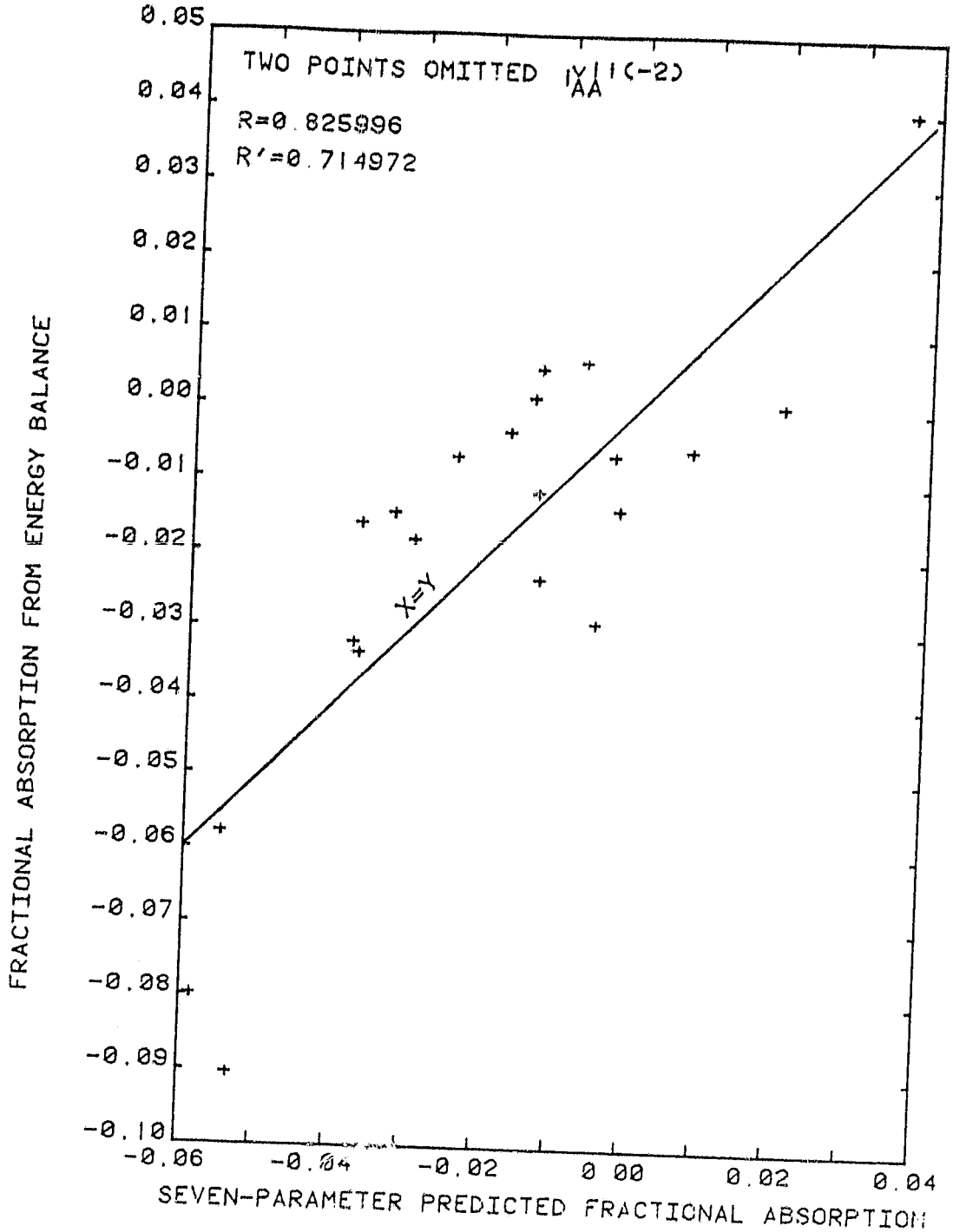

FIGURE 26. Scatter Diagram of Fractional Light Absorption by Aerosols Estimated from Energy Balance Versus Predicted Absorption for Case 1.ii(b). The Fractional light absorption by aerosols was predicted by a least-squares-fit formula derived from the data set having two cases excluded and with p 67% .

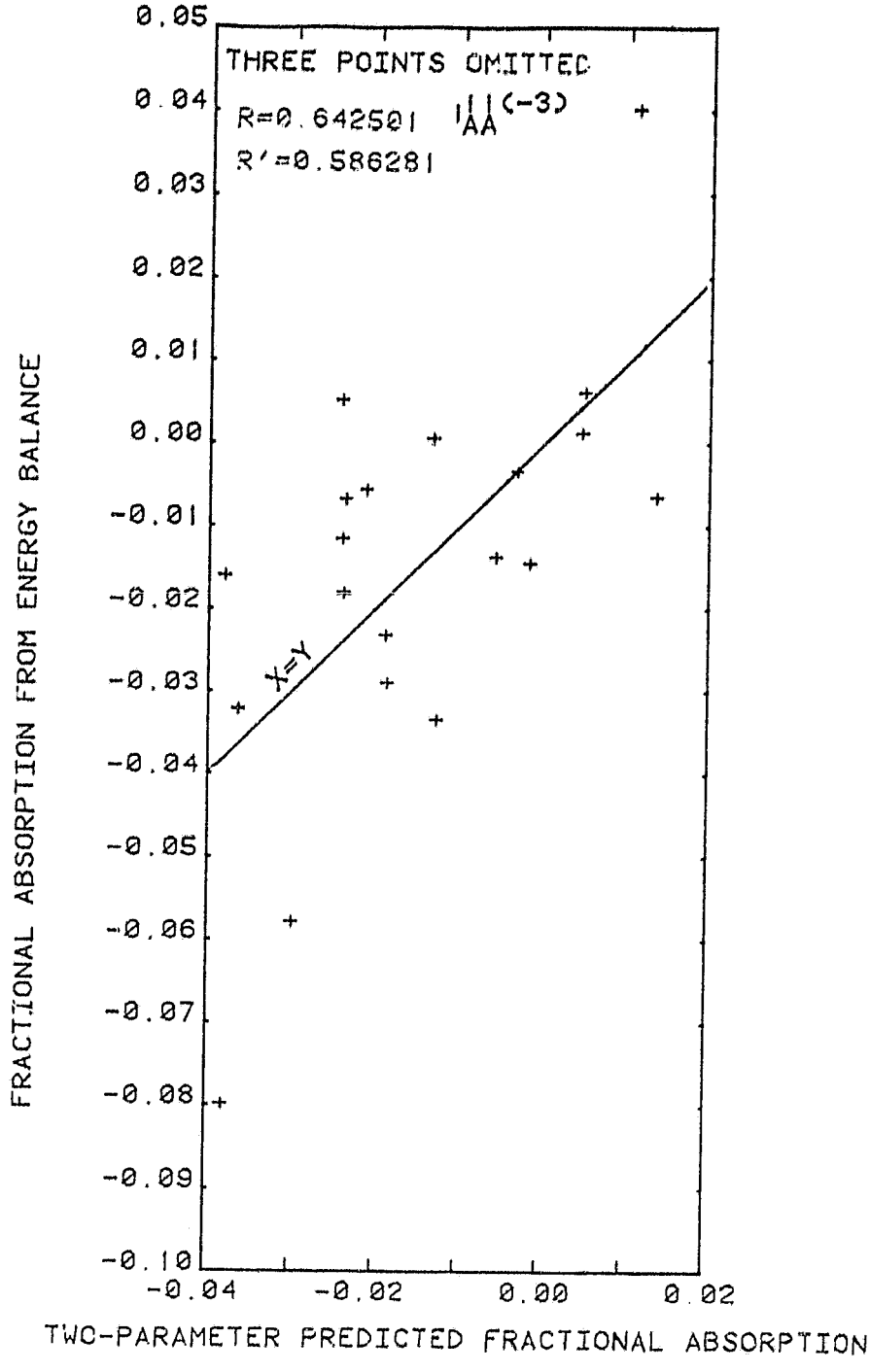

FIGURE 27. Scatter Diagram of Fractional Light Absorption by Aerosols Estimated from Energy Balance Versus Predicted Absorption for Case 2.i. The fractional light absorption by aerosols was predicted by a least-squares-fit formula derived from the data set having three cases and all turbidity related parameters excluded.

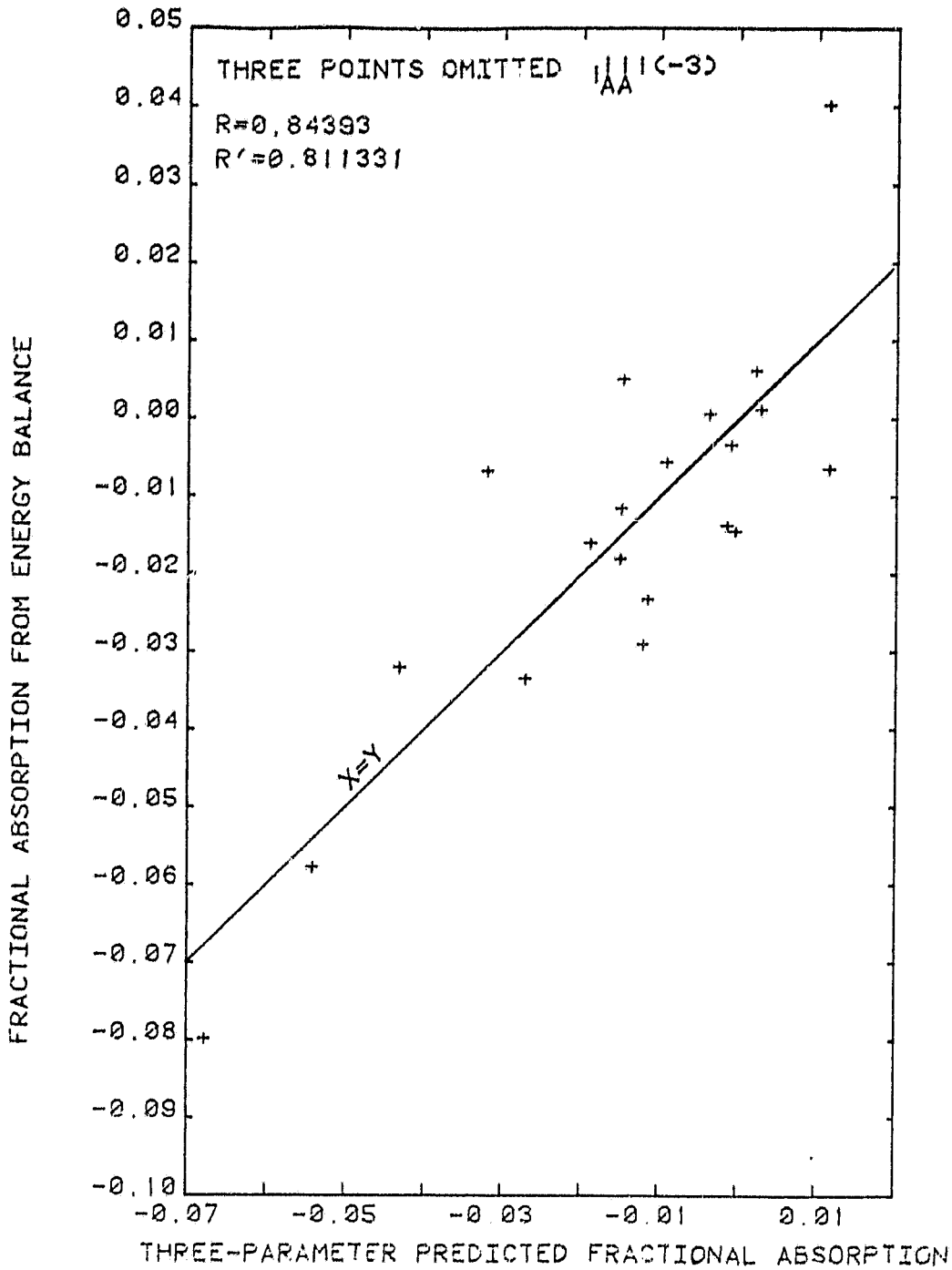

FIGURE 28. Scatter Diagram of Fractional Light Absorption by Aerosols Estimated from Energy Balance Versus Predicted Absorption for Case 2.ii. The fractional light absorption by aerosols was predicted by a least-squares-fit formula derived from the data set having three cases excluded.

REFERENCES

Ångström, A., 1961: Techniques of determining the turbidity of the atmosphere. Tellus, 13, 214-222.

Bauer, B. and J. Lienesch, 1975: VISSR data calibration. In: Bristor, C.L., 1975: NOAA Tech. Memo. NESS 64: Central Processing and Analysis of Geostationary Satellite Data. Washington, D.C., USDOC/NOAA/National Environmental Satellite Service, 155pp.

Bevington, P.R., 1969: Data Reduction and Error Analysis in the Physical Sciences. New York, San Francisco, Saint Louis, Toronto, London, McGraw-Hill Book Co., 336pp.

Blakey, R.W. and D.D. Venable, 1982: Computer automation of a solar radiation laboratory. Paper presented at the 39th Joint Annual Meeting of the National Institute of Science and Beta Kappa Chi Scientific Society, Washington, D.C., March 17-20, 1982.

Braslau, N. and J.V. Dave, 1973: Effects of aerosols on the transfer of solar energy through realistic model atmospheres. J. Appl. Meteor., 12, 601-609.

Burch, D.E., D. Gryvnak and D. Williams, 1960: OSURF Report on Project 778: The Infrared Absorption by Carbon Dioxide. Columbus, Ohio, Ohio State University Research Foundation, 88pp.

Covert, D.S., R.J. Charlson and N.E. Ahlquist, 1972: A study of the relationship of chemical composition and humidity to light scattering by aerosols. J. Appl. Meteor., 11, 968-976.

Davis, J.M. and S.K. Cox, 1981: Atmospheric Science Paper No. 338: Regional Properties of Angular Reflectance Models. Ft. Collins, Colorado, Colorado State University, Department of Atmospheric Science, 219pp.

Ellis, J.S. and T.H. Vonder Haar, 1978: Solar radiation reaching the ground from meteorological satellite data. In: AMS, 1978: Proceedings of the Third Conference on Atmospheric Radiation, June 28-30, 1978, Davis, California. Boston, Massachusetts, American Meteorological Society, 187-189.

Fitzgerald, J.W., 1975: Approximation formulas for the equilibrium size of an aerosol particle as a function of its dry size and composition and the ambient relative humidity. J. Appl. Meteor., 14, 1044-1049.

-----, W.A. Hoppel and M.A. Vietti, 1982: The size and scattering coefficient of urban aerosol particles at Washington, D.C. as a function of relative humidity. J. Atmos. Sci., 39, 1838-1852.

Glasstone, S., 1965: Sourcebook on the Space Sciences. Princeton, New Jersey, New York, Toronto, London, D. Van Nostrand Co., Inc., 937pp.

Griffin, T.J., D.A. Whitney and D.D. Venable, 1982: Development of a solar energy measurement laboratory for the study of insolation variations at Hampton, Virginia. Virginia J. Sci., 33, 146.

Hänel, G., 1972: Computation of the extinction of visible radiation by atmospheric aerosol particles as a function of the relative humidity, based upon measured properties. J. Aerosol Sci., 3, 377-386.

-----, 1976: Properties of atmospheric particles as functions of relative humidity at thermodynamic equilibrium with the surrounding moist air. Adv. Geophys., 19, 73-188.

Hickey, J.R., B.M. Alton, F.J. Griffin, H. Jacobowitz, P. Pellegrino, R.H. Maschhoff, E.A. Smith and T.H. Vonder Haar, 1982: Extraterrestrial solar irradiance variability. Two and one-half years of measurements from Nimbus-7. Solar Energy, 29, 125-128.

Hoyt, D.V., 1978: A model for the calculation of solar global insolation. Solar Energy, 21, 27-35.

-----, D.V., 1979: Theoretical calculations of the true solar noon atmospheric transmission. Appendix V in: EDIS/NCC, 1979: TD-9724: SOLMET Volume 2 -- Final Report: Hourly Solar Radiation -- Surface Meteorological Observations. Asheville, North Carolina, USDOC/NOAA Environmental Data and Information Service, National Climatic Center, 119-163.

Kasten, F., 1966: A new table and approximation formula for the relative optical air mass. Arch. Meteor. Geophys. Bioklim., B14, 206-223.

Lacis, A.A. and J.E. Hansen, 1974: A parameterization for the absorption of solar radiation in the Earth's atmosphere. J. Atmos. Sci., 31, 118-133.

Meszaros, A., 1971: On the variation of the size distribution of large and giant atmospheric particles as a function of the relative humidity. Tellus, 23, 436-440.

Muench, H.S., 1981: AFGL-TR-81-0050: Calibration of Geosynchronous Satellite Video Sensors. Project 6670. Hanscom AFB, Maine, USAFSC/Air Force Geophysics Laboratory, Meteorology Division, 25pp.

Nair, P.V.N. and K.G. Vohra, 1975: Growth of aqueous sulphuric acid droplets as a function of relative humidity. J. Aerosol Sci., 6, 265-271.

NOAA, 1979: SOLMET Volume 2 - Final Report, USDOC/NOAA National Climatic Center, Asheville, North Carolina.

Norton, C.C., F.R. Mosher, B. Hinton, D.W. Martin, D. Santek and W. Kuhlow, 1980: A model for calculating desert aerosol turbidity over the oceans from geostationary satellite data. J. Appl. Meteor., 19, 633-644.

Ostle, B., 1963: Statistics in Research (Second Edition). Ames, IA Iowa State University Press, 585pp.

Raschke, E., T.H. Vonder Haar, M. Pasternak and W.R. Bandeen, 1973: NASA TN D-7249: The Radiation Balance of the Earth-Atmosphere System from Nimbus 3 Radiation Measurements. Washington, D.C., National Aeronautics and Space Administration, 73pp.

Shettle, E.P. and R.W. Fenn, 1975: Models of atmospheric aerosols and their optical properties. In: AGARD, 1976: AGARD-CP-183: Optical Propagation in the Atmosphere. Copies of Papers Presented at the Electromagnetic Wave Propagation Panel Symposium, Lyngby, Denmark, 27-31 October. Neuilly Sur Seine, France, NATO Advisory Group for Aerospace Research and Development. Printed by: Technical Editing and Reproduction Ltd. Harford House, London. Session I, Reference #2, 16pp.

Stowe, L.L., H. Jacobowitz and V.R. Taylor, 1980: Reflectance characteristics of earth and cloud surfaces as measured by the ERB scanning channels on the Nimbus 7 satellite. Proc. International Radiation Symposium, August 11-16, Ft. Collins, Colorado, 430-432.

Volz, F.E., 1974: Economical multispectral sun photometer for measurements of aerosol extinction from 0.4 /μm to 1.6 /μm and precipitable water. Appl. Opt., 13, 1732-1733.

Vonder Haar, T.H. and J.S. Ellis, 1975: Solar energy micro climate as determined from satellite observations. In: Katz, Y.H. (Ed.): Proceedings of the Society of Photo-Optical Instrumentation Engineers, Vol. 68: Optics in Solar Energy Utilization. August 21-22, San Diego, California, Palos Verdes Estates, California, Society of Photo-Optical Instrumentation Engineers, 186pp.

Whitney, D.A. and T.J. Griffin, 1983: Solar energy measurement program at Hampton, Virginia. Prog. Solar Energy, 6, 927-932.

-----, D.D. Venable and T.J. Griffin, 1981: NASA Report No. CR164694: Local Effects of Partly-Cloudy Skies on Solar and Emitted Radiation -- First Annual Report. NASA Accession No. N81-30715. Washington, D.C., National Aeronautics and Space Administration, 66pp.

-----, -----, ----- and J.R. Foreman, 1982: NASA Report No. CR169272: Local Effects of Partly-Cloudy Skies of Solar and Emitted Radiation -- Second Annual Report. NASA Accession No. N82-31847. Washington, D.C., National Aeronautics and Space Administration, 99pp.

Yamamoto, G., 1962: Direct absorption of solar radiation by atmospheric water vapor, carbon dioxide and molecular oxygen. J. Atmos. Sci., 19, 182-188.

LIST OF APPENDICES

APPENDIX I

ABSTRACT - VIRGINIA ACADEMY OF SCIENCE PRESENTATION

ENVIRONMENTAL SCIENCES

DEVELOPMENT OF A SOLAR ENERGY MEASUREMENT LABORATORY FOR THE STUDY OF INSOLATION VARIATIONS AT HAMPTON, VIRGINIA. T. J. Griffin*, D. A. Whitney, and D. D. Venable. Dept. of Physics and Engineering Studies, Hampton Institute, Hampton, Virginia 23668.

The purpose of this three-year study is to investigate the cloud dependence of incident solar radiation at Hampton, Virginia. Solar irradiance at the Earth's surface is related to the extraterrestrial solar irradiance, to radiation absorbed and emitted by the atmosphere and clouds, and to radiation reflected by the Earth-atmosphere system. A ground-based measurement station has been established at Hampton Institute to monitor solar radiation, atmospheric emitted radiation, local cloud cover, and atmospheric turbidity. Continuous measurements of global, direct and diffuse solar radiation, and atmospheric infrared radiation are made and stored by computer. NOAA GOES-EAST satellite data are used to obtain albedo and cloud cover information.

Interim analyses performed on the data include monthly averages of global insolation, infrared radiation, and atmospheric turbidity. Global insolation has been correlated with fractional cloud cover from March 1, 1981 through February 1, 1982 using the ARL empirical model.
(Supported by NASA grant No. NAG-1-87)

APPENDIX II

ABSTRACT - AMERICAN SOLAR ENERGY SOCIETY PRESENTATION

SOLAR ENERGY MEASUREMENT PROGRAM AT HAMPTON, VIRGINIA

D. A. Whitney, T. J. Griffin and D. D. Venable

A global, diffuse and direct solar irradiance and atmospheric emittance measurement program was initiated in February 1981 at Hampton Institute, Hampton, Virginia. Beginning March 1, 1982 the integrated irradiance and emittance data were sampled on a one-minute basis and stored on magnetic tape by a microcomputer. Whole-sky photographs are used to document local cloud cover and are obtained on a regular basis. Atmospheric turbidity measurements are performed for clear-sky conditions with a Volz-type Sunphotometer.

Several types of analysis have been performed with the radiometric data. Hourly global insolation has been correlated with opaque cloud cover fraction using the Air Resources Laboratory empirical model[1]. The cloud cover fractions were obtained from three different sources: 1) analysis of satellite photoprints; 2) analysis of ground-based whole-sky photographs; and, 3) visual observations made by trained observers at nearby Langley Air Force Base[2]. Results of the comparisons for the first complete year of measurements will be presented.

Mean hourly and daily total integrated irradiance will be presented for each month since February 1981. Atmospheric turbidity data have been analyzed in terms of the Ångström turbidity parameters[3] and aerosol optical depths at 390 nm, 500 nm, and 875 nm. The results of the data analysis will be presented for the time period February 1981 through January 1983.

This research was supported through the NASA Grant # NAG 1-87.

1. NOAA, 1979: SOLMET Vol. 2., Final Report, Ashville, NC. USDOC/NOAA National Climatic Center.

2. We gratefully acknowledge the assistance of the personnel of Detachment 7, 3D Weather Squadron, Langley Air Force Base.

3. Ångström, A., 1961, "Techniques of Determining the Turbidity of the Atmosphere," Tellus XIII, 2, pp. 214-222.

APPENDIX III

CALIBRATION INSTRUMENTATION USED AT HAMPTON INSTITUTE

1. Calibration of Eppley NIP#20254E6

Standard Sensor- Eppley Model H-F Self-calibrating Cavity Pyrheliometer
Serial Number 18752

H-F Control Unit- Eppley Model 405, Serial Number 6621

NIP Output Monitor- Keithley digital multimeter, model 179-20A,
Serial Number 27764

2. Calibration of Eppley Electronic Integrators

Standard Millivolt Source- Honeywell Rubicon Potentiometer, Model #2730
Serial Number "NASA-Langley 103291"

Standard Source Monitor- Fluke Digital Voltmeter, Model #8300A
Serial Number 307
calibrated 9-10-81

Eppley Integrator Voltage/frequency monitor-
Hewlett-Packard Timer/Counter, Model 5327A
Serial Number 1120A00231
calibrated 12/83

Integrator Amplifier Gain and analog output monitor-
Keithley digital multimeter, Model 179-20A
Serial Number 27764

APPENDIX IV

DATA ACQUISITION AND STORAGE HARDWARE

ITEM DESCRIPTION	QUANTITY	MANUFACTURER & MODEL NUMBER
Integrator with BCD Interface	4	Eppley Laboratory, Model 411-6140
Microcomputer System with RS232 Interface	2	Tektronix, Inc., Model 4051
Microcomputer ROM Expander	1	Tektronix, Inc., Model 4051E01
Real Time Clock ROM Pack	1	Trans Era, Model 641-RTC
Binary/BCD I/O Interfaces - Interconnected - User Supplied Interface Box	5	Trans Era, Model 632 BCD with Options 1 and 2
Minicomputer with 9 Track Tape Drive	1	Digital Equipment, PDP 11/34
Interface Box with LED Photo Count Display	1	Designed and Built by D. D. Venable & R. W. Blakey
2 Channel - 12 Bit D/A Converter *	1	Trans Era, Model 620 DAC
12 Bit 16 Channel Data Acquisition System *	1	Trans Era, Model 652 ADC

* These two devices were used in the design and testing stages.

APPENDIX V

ABSTRACT - BETA KAPPA CHI PRESENTATION

COMPUTER AUTOMATION OF A SOLAR RADIATION LABORATORY. R. W. Blakey* and D. D. Venable, Physics Department, Hampton Institute, Hampton, VA 23668

A solar radiation measurement laboratory that includes two precision spectra pyranometers, a precision infrared radiometer, a normal incidence pyrheliometer and an all sky camera has been automated to allow direct computer acquisition of insolation data. Signals from the solar instruments are integrated and displayed on five digit light-emitting-diode displays. The integrated signals are transferred via a general purpose interface card to a microcomputer. We have designed, constructed and implemented hardware and software configurations that permit data acquisition, storage, transfer, and display. System reliability tests have been performed and mean time between failure and system down time have been characterized.

APPENDIX VI

ESTIMATION OF VISSR UNCERTAINTY

An uncertainty of 20%, in the calibration and digitization of full-resolution visual imagery, was obtained using the following reasoning:

Assume that the 5 x 5 image array used in estimating the spaceward reflectance of the Earth-atmosphere system is about 3/5 land (reflectance $\tilde{=}$ 0.15) and 2/5 water (reflectance $\tilde{=}$ 0.04) for the local solar measurement site geography using Table 7 in Muench (1981); the net random error, after multiplying the land and ocean reflectivities by the weights just given, for this array is 9.8% for 1 mi x 1 mi resolution. Assuming that the inverse proportionality between the net random error and the nadir-point resolution holds between ½ mi x ½ mi and 1 mi x 1 mi as it does between 1 mi x 1 mi and 4 mi x 4 mi, this translates to a net random error of 19.6% for ½ mi x ½ mi. The pythagorean sum of this with the 5% systematic calibration errors for the variable model of Muench (1981) yields 20.2% which should be rounded to 20%.